



# On the origin of magnetic driven winds and the structure of the galactic dynamo in isolated galaxies

Ulrich P. Steinwandel,<sup>1,2</sup>★ Klaus Dolag,<sup>1,2</sup> Harald Lesch,<sup>1</sup> Benjamin P. Moster<sup>1,2</sup>, Andreas Burkert<sup>1,3</sup> and Almudena Prieto<sup>4,5</sup>

<sup>1</sup>*Fakultät für Physik, Universitäts-Sternwarte München, LMU Munich, Scheinerstr 1, D-81679, Germany*

<sup>2</sup>*Max Planck Institute for Astrophysics, Karl-Schwarzschild-Str 1, D-85741 Garching, Germany*

<sup>3</sup>*Max Planck Institute for Extraterrestrial Physics, Giessenbachstr 1, D-85748 Garching, Germany*

<sup>4</sup>*Instituto de Astrofísica de Canarias, Vía L'actea, La Laguna (Tenerife), E-38205, Spain*

<sup>5</sup>*Departamento de Astrofísica, Universidad de La Laguna, Avenida Astrofísico Francisco Sánchez, San Cristóbal de La Laguna (Tenerife), E-38200, Spain*

Accepted 2020 March 4. Received 2020 March 3; in original form 2019 July 29

## ABSTRACT

We investigate the build-up of the galactic dynamo and subsequently the origin of a magnetic driven outflow. We use a set-up of an isolated disc galaxy with a realistic circum-galactic medium (CGM). We find good agreement of the galactic dynamo with theoretical and observational predictions from the radial and toroidal components of the magnetic field as function of radius and disc scale height. We find several field reversals indicating dipole structure at early times and quadrupole structure at late times. Together with the magnetic pitch angle and the dynamo control parameters  $R_\alpha$ ,  $R_\omega$ , and  $D$ , we present strong evidence for an  $\alpha^2 - \Omega$  dynamo. The formation of a bar in the centre leads to further amplification of the magnetic field via adiabatic compression which subsequently drives an outflow. Due to the Parker instability the magnetic field lines rise to the edge of the disc, break out, and expand freely in the CGM driven by the magnetic pressure. Finally, we investigate the correlation between magnetic field and star formation rate. Globally, we find that the magnetic field is increasing as function of the star formation rate surface density with a slope between 0.3 and 0.45 in good agreement with predictions from theory and observations. Locally, we find that the magnetic field can decrease while star formation increases. We find that this effect is correlated with the diffusion of magnetic field from the spiral arms to the interarm regions which we explicitly include by solving the induction equation and accounting for non-linear terms.

**Key words:** methods: numerical – galaxies: evolution – galaxies: formation – galaxies: general – galaxies: magnetic fields.

## 1 INTRODUCTION

Magnetic fields are a quantity of paramount importance in the Universe. Their influence ranges from the interior of the earth and the sun over interactions with dust in proto planetary and proto stellar discs to molecular clouds and finally galaxies, galaxy clusters, and the large-scale structure of the Universe.

Observationally, there are a few common tracers to quantify the presence of magnetic fields in the nearby Universe, like the radio synchrotron emission and its polarization along the line of sight, the Faraday rotation measure or the Zeeman-splitting of star light within galaxies. Using these methods the magnetic

field strengths of nearby galaxies are very well constrained. By assuming that the magnetic field is in equipartition with the other energetic components of a galaxy, the magnetic field strength can be determined to a few  $\mu\text{G}$  (e.g. Niklas et al. 1995; Fletcher 2010). Higher magnetic field strengths up to 50  $\mu\text{G}$  are observed in the spiral arms of galaxies (e.g. Beck 2015; Han 2017). The highest magnetic fields can be found in starburst galaxies (Chyžík et al. 2003; Beck 2005; Heesen et al. 2011) or in the galactic centre (e.g. Robishaw, Quataert & Heiles 2008) and can reach values up to 1 mG. There is observational evidence that the energy density generated by the magnetic field can be dynamically important. Beck (2007), Tabatabaei et al. (2008), and Basu & Roy (2013) find in different galaxies that the magnetic energy density can be in the same order of magnitude as the energy density induced by the turbulent motions within the interstellar medium (ISM), indicating that the ISM is a

\* E-mail: [usteinw@usm.lmu.de](mailto:usteinw@usm.lmu.de)

low  $\beta$ -plasma where  $\beta$  is the ratio between thermal and magnetic pressure.

The morphology of magnetic fields can be investigated by the emission of synchrotron radiation in spiral galaxies. The results indicate that the magnetic fields of spiral galaxies can show a spiral structure itself which is especially prominent in so-called grand design spiral galaxies like M51 and M83 (Patrikeev et al. 2006; Beck et al. 2013; Houde et al. 2013). In spiral galaxies with strong density wave structure, the magnetic fields morphology is often tightly bound to the spiral structure of the density waves. However, if the density waves are sub-dominant the large-scale ordered magnetic fields do not necessarily align with the spiral structure of the gaseous arms (Beck 2015; Han 2017). Faraday rotation measurements of polarized sources in the radio continuum can be utilized to determine the morphology and the strength of magnetic fields in nearby spiral galaxies and the Milky Way (e.g. Han et al. 2018). However, the Faraday rotation measure is a not single valued estimate of the magnetic field structure if there are various sources with different rotations and a variety of internal structure. In these cases, the physical meaning of the RM measurements remains unclear, and the RM measurements can be replaced by the Faraday depth (Rotation measure synthesis) method to obtain information about the magnetic field strength and structure (e.g. Burn 1966; Brentjens & de Bruyn 2005; Heald et al. 2015; Sun et al. 2015; Kim et al. 2016). To interpret and understand the data obtained from these methods, it is important to build detailed theoretical models that lead to a more detailed picture of the physical interpretation.

Further, the magnetic field can play an important role in regulating the star formation process on galactic scales. In observations, it has been observed that the total magnetic field strength is directly correlated with the star formation rate (SFR) density with a power-law scaling exponent that is measured between 0.18 (Chyží et al. 2007) and 0.3 (Heesen et al. 2014). However, recent observations of molecular clouds in NGC 1097 indicate that locally the star formation surface density might also show an anticorrelation with increasing magnetic field (Tabatabaei et al. 2018).

Although the field strengths of magnetic fields in nearby galaxies are very well known, the origin of those magnetic fields is still under debate. It is possible to generate tiny seed fields with  $10^{-20}$  G via the Biermann-battery process (e.g. Biermann 1950; Mishustin & Ruzmaikin 1972; Zeldovich, Ruzmaikin & Sokolov 1983) or by phase transitions in the early universe (e.g. Hogan 1983; Ruzmaikin, Sokolov & Shukurov 1988a, b; Widrow 2002). Once these seed fields are present, they can be amplified via different dynamo processes. The three major ones are given by the cosmic ray driven dynamo (Lesch & Hanasz 2003; Hanasz et al. 2009), the  $\alpha$ - $\Omega$  dynamo (Ruzmaikin et al. 1979) and the small-scale turbulent dynamo (Kazantsev 1968; Kraichnan 1968; Kazantsev, Ruzmaikin & Sokolov 1985). While the cosmic ray driven dynamo and the  $\alpha$ - $\Omega$  dynamo operate close to Gyr time-scales the small-scale turbulent dynamo operates on Myr time-scales and can therefore lead to a rapid growth of the magnetic field on short galactic time-scales. In the small-scale turbulent dynamo, the magnetic field lines are stretched, twisted, and folded due to turbulence on the smallest scales in the ISM, which leads to an amplification of the magnetic field. The field is then regulated by random motion on the larger scales (Zeldovich et al. 1983; Kulsrud & Anderson 1992; Kulsrud et al. 1997; Malyshkin & Kulsrud 2002; Schekochihin et al. 2002, 2004; Schleicher et al. 2010). The turbulence on the smallest scales can be driven by various physical processes with SN-feedback being the most prominent one (e.g. Elmegreen & Scalo 2004). Further, theoretical calculations can predict the structure of the magnetic

field which turns out to be either dipolar or quadrupolar (Shukurov et al. 2019), whereby the quadrupolar structures decay faster if the dynamo action is switched off. The field structure can then be determined by the symmetry of the magnetic field around the mid-plane, where uneven symmetry determines a dipolar field while even symmetry indicates a quadrupolar field.

Recently, there have been various simulations of isolated galaxies, cosmological zoom-in simulations, and larger cosmological volumes that include a prescription for solving the equations of magneto hydrodynamics. These simulations provide strong evidence for a small-scale turbulent dynamo on scales of galaxies (Beck et al. 2012; Pakmor & Springel 2013; Rieder & Teyssier 2016; Butsky et al. 2017; Pakmor et al. 2017; Rieder & Teyssier 2017; Steinwandel et al. 2019) and galaxy clusters (Dolag, Bartelmann & Lesch 1999; Dolag et al. 2001; Xu et al. 2009; Vazza et al. 2018; Roh et al. 2019). All of these simulations find indications in the magnetic power spectra for small-scale turbulence driven amplification of the magnetic field. The origin of the turbulence on the small-scales is in all cases mostly dominated by the feedback of supernovae (SNe; e.g. Somerville & Davé 2015; Naab & Ostriker 2017).

Pakmor & Springel (2013) and Steinwandel et al. (2019) discuss the possibility of outflows that are driven by the magnetic pressure only, finding a slight decrease in the SFRs in systems that are more massive than  $10^{10}$  M<sub>⊙</sub>. Both studies note that the condition for magnetic outflows is given if the magnetic pressure is dominating over the thermal pressure of the galaxy. Low-mass systems are only weakly influenced by magnetic outflows because the amplification process of the magnetic field is merely inactive due to shallow potential wells and the low SFR that leads to a small amount of SNe and therefore no source for small-scale turbulence (apart from accretion shocks). Moreover, the  $\alpha$ - $\Omega$  dynamo is not contributing much to the amplification of the magnetic field, but can order the field on larger scales. In the higher mass systems there is a magnetic driven wind which has the potential to contribute as an additional feedback process to the matter cycle within galaxies. Usually, there are two main sources that can drive galactic outflows that are well studied in both observations and simulations and regulate the baryon cycle in galaxies, namely SN-feedback and the feedback of active galactic nuclei (AGNs).

This paper is structured as follows. In Section 2, we present some of the fundamental findings of galactic dynamo theory. In Section 3, we present the simulation suite that we use for our analysis alongside with the galactic model and the applied physics modules. In Section 4, we investigate the origins and the properties of magnetic driven winds. In Section 5, we discuss the results, presenting different properties from the dynamo theory. In Section 6, we discuss the correlation between the magnetic field and the SFR. Finally, we present a summary of our work alongside with the conclusions and limits of the model in Section 7.

## 2 FUNDAMENTALS OF DYNAMO THEORY

As the magnetic field is enhanced by the acting galactic dynamo, we can follow the build-up of its structure. The fundamentals of dynamo theory can be derived from the induction equation of magnetohydrodynamics (MHD).

$$\frac{\partial \mathbf{B}}{\partial t} = \nabla \times (\mathbf{v} \times \mathbf{B}) - \nabla \times \eta(\nabla \times \mathbf{B}), \quad (1)$$

where  $\eta$  is the magnetic resistivity,  $\mathbf{B}$  the magnetic field, and  $\mathbf{v}$  the gas velocity. Regarding this equation, magnetic fields can be amplified when small magnetic seed fields are twisted by fluid

flows. In classical MHD, the magnetic field is tightly coupled to the movement of the gas. In this picture, the galaxy provides the large-scale velocity structure due to differential rotation of the disc. Therefore, the understanding of the velocity structure of a galaxy can lead to the understanding of the build-up of the magnetic field within the galaxy. In spiral galaxies, the gas is rotating differentially within the potential that is provided by the dark matter halo of the galaxy and its stellar disc and bulge. Various processes like bar-instabilities or tidal forces due to gravitational interaction, in spiral galaxies transport angular momentum outwards and mass inwards. Therefore, the centre of the galaxy is constantly provided with gas that moves towards the centre. This gas cools, forms stars, and eventually generates feedback by starburst driven winds or winds driven by the feedback of SNe which can lead to enrichment of the galactic halo. In disc galaxies, the dominant component of the velocity is given as the axis symmetric rotation with usually only very small velocity components perpendicular to the galactic disc (which can be interpreted as the turbulent motion of the fluid). This rotational velocity structure of the galactic disc is therefore highly complicated but its evolution is tightly coupled to the large-scale components of the galaxy, like its dark matter halo, the stellar disc, and the bulge.

Apart from the large-scale velocity structure of the galaxy, small-scale perturbations in the velocity can be generated by various feedback processes within the ISM (e.g. stellar wind feedback, SN-feedback, collisions of molecular clouds, feedback of active galactic nuclei) which stir the gas and introduce small-scale vertical motions that lead finally to the build-up of ISM-MHD turbulence. This introduces two effects that have to be considered to understand the build-up of magnetic fields in spiral galaxies. The first one is the so-called helicity (convective turbulent motion of the gas, perpendicular to the disc) which enhances the magnetic field strength and supports the galactic dynamo. The second one is the turbulent diffusion which leads to a loss of magnetic energy due to (partially) reconnecting magnetic field lines. In this process magnetic energy that is carried by the magnetic field lines is converted into thermal energy. Therefore, this process works against the galactic dynamo. By including the small-scale perturbations that are introduced over various feedback processes in the ISM one can derive the mean field dynamo equation following for example Wielebinski & Krause (1993), Sur, Shukurov & Subramanian (2007), and Brandenburg (2009). Within the scope of the mean field dynamo the velocity field and the magnetic field can be written as follows:

$$\mathbf{v} = \langle \mathbf{v} \rangle + \mathbf{v}^{(1)}, \quad (2)$$

$$\mathbf{B} = \langle \mathbf{B} \rangle + \mathbf{B}^{(1)}, \quad (3)$$

where  $\mathbf{v}^{(1)}$  and  $\mathbf{B}^{(1)}$  denote the small-scale fluctuations of the velocity field and the magnetic field, respectively. The small-scale fluctuations in the velocity field are locked to the small-scale fluctuations in the magnetic field and coupled via  $\nabla \times \alpha(\mathbf{B})$  with  $\alpha$  given by Zeldovich et al. (1983) via  $\frac{1}{3}\tau(\mathbf{v}^{(1)} \cdot (\nabla \times \mathbf{v}^{(1)}))$  and  $\eta_T \Delta(\mathbf{B})$ , where  $\eta_T$  is the turbulent diffusion coefficient. It is directly proportional to the turbulent length-scale  $l_{\text{turb}}$  and the turbulent velocity  $v_{\text{turb}}$ . This leads to the dynamo equation given by

$$\frac{\partial \mathbf{B}}{\partial t} = \nabla \times (\mathbf{v} \times \mathbf{B}) + \nabla \times \alpha \mathbf{B}. \quad (4)$$

We assume that the magnetic diffusivity is small and not strongly dependent on the environment. However, this is a rough approximation that breaks down in strong shocks that give an upper limit on the magnetic field amplification. In this picture, the magnetic

field is amplified in a two-stage process. First the radial component  $B_r$  is amplified via small-scale radial motion (convective turbulence and/or buoyancy). In the second step,  $B_\varphi$  is generated via the  $\Omega$ -effect (large scale rotation of the axis-symmetric component) from  $B_r$ . This behaviour can be directly seen from writing down the rate of change of the single magnetic field components in cylindrical coordinates given as

$$\begin{aligned} \frac{\partial B_r}{\partial t} = & -B_r \frac{v_r}{r} - \frac{1}{r} B_r \frac{\partial v_\varphi}{\partial \varphi} - B_r \frac{\partial v_z}{\partial z} + \frac{1}{r} B_\varphi \frac{\partial v_r}{\partial \varphi} \\ & + B_z \frac{\partial v_r}{\partial z} - v_r \frac{\partial B_r}{\partial r} - \frac{v_\varphi}{r} \frac{\partial B_r}{\partial \varphi} - v_z \frac{\partial B_r}{\partial z}, \end{aligned} \quad (5)$$

$$\begin{aligned} \frac{\partial B_\varphi}{\partial t} = & -B_\varphi \frac{\partial v_r}{\partial r} - B_\varphi \frac{\partial v_z}{\partial z} + B_r \frac{\partial v_\varphi}{\partial r} + B_z \frac{\partial v_\varphi}{\partial z} \\ & - v_r \frac{\partial B_\varphi}{\partial r} - \frac{v_\varphi}{r} \frac{\partial B_\varphi}{\partial \varphi} - v_z \frac{\partial B_\varphi}{\partial z} - v_\varphi \frac{\partial B_r}{\partial r}, \end{aligned} \quad (6)$$

$$\begin{aligned} \frac{\partial B_z}{\partial t} = & -B_z \frac{v_r}{r} - B_z \frac{\partial v_r}{\partial r} - \frac{1}{r} B_z \frac{\partial v_\varphi}{\partial \varphi} + B_r \frac{\partial v_z}{\partial r} \\ & + \frac{1}{r} B_\varphi \frac{\partial v_z}{\partial \varphi} - v_r \frac{\partial B_z}{\partial r} - \frac{v_\varphi}{r} \frac{\partial B_z}{\partial \varphi} - v_z \frac{\partial B_z}{\partial z}. \end{aligned} \quad (7)$$

If we assume the system of interest to be a razor thin, differentially rotating galactic disc then we can cross out some terms from the above equations. Because differentially rotating systems have a flat rotation curve, all terms with  $\partial v_\varphi / \partial r$  cancel out. Further, we can assume axis symmetry for the velocity. This means that the velocity is independent of the angle  $\varphi$  and a vanishing magnetic field in  $z$ -direction. The magnetic field within the disc can then be written as follows

$$\frac{\dot{\partial} B_r}{\partial t} = -B_r \frac{v_r}{r}, \quad (8)$$

$$\frac{\partial B_\varphi}{\partial t} = -B_\varphi \frac{\partial v_r}{\partial r} - v_\varphi \frac{B_r}{r} = B_\varphi \frac{\partial v_r}{\partial r} + r B_r \frac{\partial \Omega}{\partial r}, \quad (9)$$

with the angular velocity  $\Omega$ . From the last term of equation (9), we directly see that a toroidal field is generated from an already existing radial field by the large-scale rotation of the galactic disc. This effect is limited when all of the radial field is wound up and therefore has been converted into a toroidal field. However, due to radial inflow the radial field can be compressed and subsequently amplified. Due to the  $\Omega$ -effect this radially amplified magnetic field can again be converted into a toroidal field and the process continues until the equipartition field strength is reached and the dynamo saturates.

### 3 SIMULATIONS

#### 3.1 Simulation code

All presented simulations are carried out with the Tree SPMHD code GADGET-3 (Springel 2005a). GADGET-3 solves the equations of Newtonian gravity via a Tree code (Barnes & Hut 1986). The fluid equations are solved with a particle ansatz utilizing the smoothed particle hydrodynamics (SPH) method. We use a modern version of SPH that is presented in Beck et al. (2016) with artificial viscosity and conduction terms to overcome known problems of the method in terms of shock-capturing and fluid mixing instabilities (Agertz et al. 2007; Junk et al. 2010). The details of the implementation of the magnetohydrodynamics version is presented in Dolag & Stasyszyn (2009) and has been used successfully in different studies (e.g. Kotarba et al. 2011; Beck et al. 2012, 2013; Geng et al. 2012a, b; Steinwandel et al. 2019). We are aware of the divergence cleaning constraints that can be problematic in particle methods. Therefore,

**Table 1.** Number of particles, mass resolution, and gravitational softening lengths for our three galactic systems.

	Particle numbers ( $10^6$ )			
	DW	MM	MW	
Gas disc	$N_{\text{gd}}$	0.8	1.0	1.2
Gas halo	$N_{\text{gh}}$	5.0	6.0	7.0
Stellar disc	$N_{\text{sd}}$	3.2	4.0	4.8
Stellar bulge	$N_{\text{b}}$	1.3	1.6	2.0
Dark matter	$N_{\text{dm}}$	4.6	5.7	6.9
Mass resolution ( $M_{\odot}$ )		DW	MM	MW
Gas particles	$m_{\text{gas}}$	72	510	4800
Star particles	$m_{\text{star}}$	72	510	4800
Dark matter	$m_{\text{dm}}$	1440	10200	96000
Gravitational softening (pc)		DW	MM	MW
Gas particles	$\epsilon_{\text{gas}}$	5	10	20
Star particles	$\epsilon_{\text{star}}$	5	10	20
Dark matter	$\epsilon_{\text{dm}}$	40	20	10

**Table 2.** Adopted parameters for our three galactic systems.

	Disc parameters			
	DW	MM	MW	
Total mass ( $10^{10} M_{\odot}$ )	$M_{200}$	1	10	100
Virial radius (kpc)	$r_{200}$	31	67	145
Halo concentration	$c$	8	10	12
Spin parameter	$\lambda$	0.033	0.033	0.033
Disc mass fraction	$m_d$	0.041	0.041	0.041
Bulge mass fraction	$m_b$	0.013	0.013	0.013
Disc spin fraction	$j_d$	0.041	0.041	0.041
Gas fraction	$f$	0.2	0.2	0.2
Disc scale length (kpc)	$l_d$	0.8	1.5	2.1
Disc height	$z_0$	$0.2 l_d$	$0.2 l_d$	$0.2 l_d$
Bulge size	$l_b$	$0.2 l_d$	$0.2 l_d$	$0.2 l_d$

we use a divergence cleaning method following Powell et al. (1999). For the presented set of simulations, we showed in Steinwandel et al. (2019) that the magnetic energy density stays below the kinetic energy density for all times within the simulation by at least a factor of 100, proofing the Powell et al. (1999) cleaning scheme to be sufficient for the purpose at hand. We note that we tested the Dedner et al. (2002) cleaning scheme on the Milky Way like models showing little differences. This is expected as the simulations have quite high resolution and large differences in the cleaning scheme are only expected at low resolution with the Dedner et al. (2002) cleaning scheme being more diffusive than the Powell et al. (1999) cleaning scheme.

### 3.2 Galactic model

We use the Milky Way like model of the set of simulations that are presented in Steinwandel et al. (2019). This set consists out of three galaxies with halo masses  $10^{10}$  (DW),  $10^{11}$  (MM), and  $10^{12} M_{\odot}$  (MW) with an explicit modelled circum-galactic medium (CGM) that is motivated by observations of the CGM of the Milky Way (Miller & Bregman 2013) for the  $10^{12} M_{\odot}$  galaxy. We show the specifics of all models in Tables 1–3 in terms of particle numbers, disc parameters, and CGM properties. The CGMs for the lower mass galaxies are scaled down versions of the high-mass model for the sake of simplicity. This model gives us the advantage to

**Table 3.** Parameters for the gaseous halo.

	General parameters			
	DW	MM	MW	
Total mass ( $10^{10} M_{\odot}$ )	$M_{\text{gh}}$	0.05	0.5	5.0
Virial temperature (K)	$T_{\text{vir}}$	$10^4$	$10^5$	$10^6$
Settings for the $\beta$ -model				
Exponent	$\beta$		2/3	
Density in ( $\text{g cm}^{-3}$ )	$\rho_0$		$5 \cdot 10^{-26}$	
Core radius	$r_c$	$0.22 \cdot r_s$	$0.25 \cdot r_s$	$0.33 \cdot r_s$

provide accretion from the CGM to the disc and allows detailed studies of the interaction between the disc and the CGM in a controlled environment. We utilize two different implementations of the magnetic field. In the first one, a primordial magnetic field of  $10^{-9}$  G is applied in  $x$ -direction (denoted with the identifier *primB* if used). We note that the equatorial plane is in the  $x$ – $y$  plane. In the second one, the magnetic field is coupled to the SN explosions and seeds a magnetic dipole in a certain region around an exploding star. For the model details, we refer to Beck et al. (2013). This model is indicated with the identifier *snB*. As we find almost no difference in the structure of the magnetic field and the dynamical behaviour of the galaxy between the models *primB* and *snB* we only perform the analysis of the more realistic model *snB* and comment on the (slight) differences within the model *primB* if necessary. For completeness we show all the necessary parameters for all disc and CGM properties in the whole simulation set in Tables 1–3.

All galaxies consist out of a dark matter halo that is modelled via a Hernquist profile (Hernquist 1993) a bulge, a stellar disc, and a gas disc that is consisting out of SPH particles. While the bulge is following a Hernquist profile, the stellar and the gas disc follow exponential surface density profiles that are motivated by observations. These components are modelled with the method that is presented in Springel (2005b) with explicitly modelled particle profiles for all components of the galaxy. The CGM is modelled separately as a  $\beta$ -profile (Cavaliere & Fusco-Femiano 1978) as SPH particles from a glass-distribution with the given radial density in spherical coordinates:

$$\rho(r) = \left(1 + \frac{r^2}{r_c^2}\right)^{\frac{3}{\beta}}. \quad (10)$$

The method that is used to build the galactic model is presented in detail in Steinwandel et al. (2019) and follows similar implementations on galactic scales (e.g. Moster et al. 2010) and cluster scales (e.g. Donnert 2014). However, we note that we introduced some small modifications to these models to fit the environment of isolated galaxies without perturbing the original system. We illustrate the model in Fig. 1. With this model it is possible to simulate a Milky Way like galaxy with the focus on resolving the galactic dynamo. We show an example of the resulting galactic system in Fig. 2.

### 3.3 Previous work

In Steinwandel et al. (2019), we already discussed the amplification processes for the magnetic field that we can resolve in our simulations and find strong evidence for three processes, adiabatic compression, the  $\alpha$ – $\Omega$  dynamo, and the small-scale turbulent dynamo and showed agreement with other work (e.g. Rieder & Teyssier 2016; Pakmor et al. 2017; Vazza et al. 2018). We identified the regimes of adiabatic compression via the scaling law  $B \propto \rho^{2/3}$

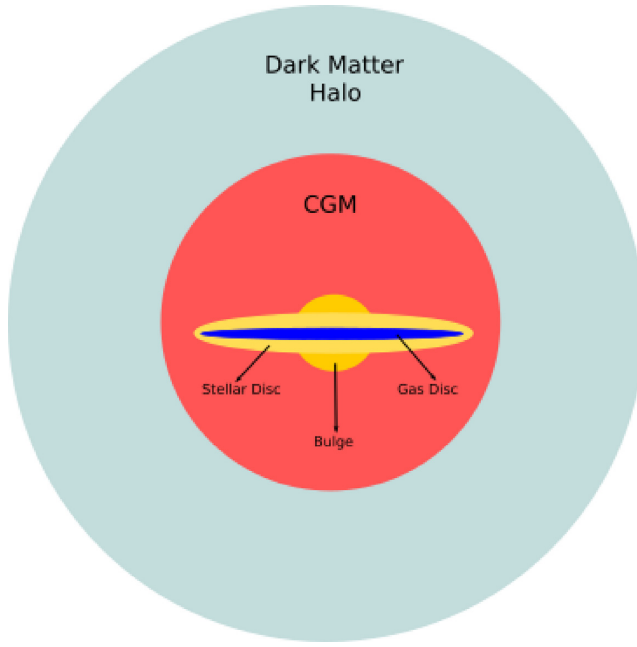


**Figure 1.** Schematic sketch of the galactic model we employ. The system is consisting out of a stellar disc (light yellow), a stellar bulge (dark yellow), a cold gas disc (blue), and a hot CGM (red). The whole system is embedded in a large dark matter halo (light blue).

which can be obtained from the flux freezing argument of ideal MHD that states that the magnetic flux through the surface of a collapsing gas cloud is constant. The magnetic field can then only be amplified due to collapse perpendicular to the magnetic field lines. We identified the  $\alpha-\Omega$  over the large-scale rotation of the galactic disc. The small-scale turbulent dynamo could be identified by the power-law slope that is predicted via Kazantsev (1968) in the low-magnetic power regime. Turbulence is driven on the scales of a few 100 pc due to SN-feedback and leads to small scale turbulent motion (similar to the  $\alpha$  effect). We further found this process in the behaviour of the curvature of the magnetic field lines in good agreement with the results of Schekochihin et al. (2004). While these quantities are a good observable for comparison with dynamo theory they cannot straight forward be obtained from observations. However, there are a few observables that can quantify the dynamo process and the higher order structure of the magnetic field that can be observed, which we will discuss in Section 5. Further, we probed the effect of the magnetic driven outflow as a function of time on the SFR and found that the SFR is reduced by 40 per cent in the presence of magnetic field compared to a reference simulation that does not incorporate magnetic fields (Steinwandel et al. 2019). Further we find a mass outflow rate of a 0.5 solar masses (peak outflow rate) with a saturation value of roughly around zero solar masses per year, once an equilibrium between outflow rate and accretion rate is established. We show this behaviour in Fig. 3 where we show the mass budget of the galactic disc as a function of time. We compare our fiducial SN-seeding model (red line) with a model that does not include the effects of MHD (black line). While we find that the peak outflow rate is too low compared to the outflow rate of the Milky Way or even compared to galaxies at high redshift, the effect could still be of importance. At very high redshift, when galaxies mainly grow due to smooth accretion and SN feedback is not yet dominating, magnetic driven outflows could delay star formation and thus contribute to the quenching of the first galaxies

by internally regulating their star formation efficiencies. Moreover, it is expected that the outflow properties are set by all thermal and non-thermal components of the ISM and not by the magnetic field alone (e.g. cosmic rays). The interplay of all these components has to be studied in future simulations.

## 4 BAR FORMATION AND MAGNETIC DRIVEN OUTFLOWS

### 4.1 Formation of the magnetic driven outflow

In Steinwandel et al. (2019), we discussed the possibility of outflows that are driven by the magnetic field alone. Due to the amplification of the weak magnetic field in the beginning of the simulation, the system is in a high-plasma  $\beta$  regime. In this regime, the system is completely supported by the thermal pressure in the disc and the magnetic field has no dynamic impact on the structure of the ISM. At later times, when the plasma  $\beta$  is of the order of 1 and the magnetic pressure is of the same order of magnitude as the thermal pressure (or even higher) the magnetic field becomes dynamically important and can launch a highly magnetized, weak wind into the outer regions of the surrounding CGM. The gas is accelerated to a few  $100 \text{ km s}^{-1}$  during this process. In the following, we want to describe the launch process of the wind in more detail. It is a combination of the acting small-scale turbulent dynamo in the innermost kpc of the disc, adiabatic compression of the field lines, the acting Parker instability<sup>1</sup> that lifts the magnetic field lines above the disc within a few 100 Myr and the formation process of a bar which is destabilizing the central region of the galaxy. The launching process can be subdivided in four stages.

(i) Small-scale turbulent dynamo: The magnetic field in the centre of the galaxy is amplified via the small-scale turbulent dynamo. The small-scale turbulence is induced by SN-feedback and accretion shocks generated by the in falling gas from the CGM. The central regions of the galaxy have the highest SFRs and subsequently the highest SN rates. The turbulence in the central region leads to more effective star formation and amplifies the magnetic field further. However, the amplification process of the magnetic field over the dynamo saturates at a few  $10 \mu\text{G}$  in the centre.

(ii) Bar formation: At around 1.8 Gyr the galaxy starts to form a bar in the innermost kpc. Due to the high SFR in this region, the gas is quickly depleted, leading to the radial gas in-fall due to the steep potential wells of the dark matter potential in Milky Way like galaxies. Subsequently this leads to the formation of a bar, which gravitationally destabilizes the central region of the galaxy.

(iii) Mass accretion through the bar: Once the bar has formed the central region of the galaxy can quickly accrete mass by transporting mass along the bar towards the centre while angular momentum is deposited in the outer region of the bar. The magnetic field can then be amplified by adiabatic compression if there is a mass flux perpendicular to the magnetic field lines and reach values of a few  $10 \mu\text{G}$  in the very centre of the galaxy.

(iv) Buoyancy Instability: Finally, magnetic field lines are moving upwards (or downwards) driven by the Parker or buoyancy instability. Due to the density gradient in  $z$ -direction of the disc, the

<sup>1</sup>The fastest growing mode of the Parker instability is proportional to the disc scale height. Therefore, to resolve the Parker Instability one has to resolve the disc scale height in the simulation. As our resolution is 10 pc (limited by the gravitational softening), we resolve the disc scale height of roughly 200 pc well enough to capture the buoyancy driven Parker lobes.

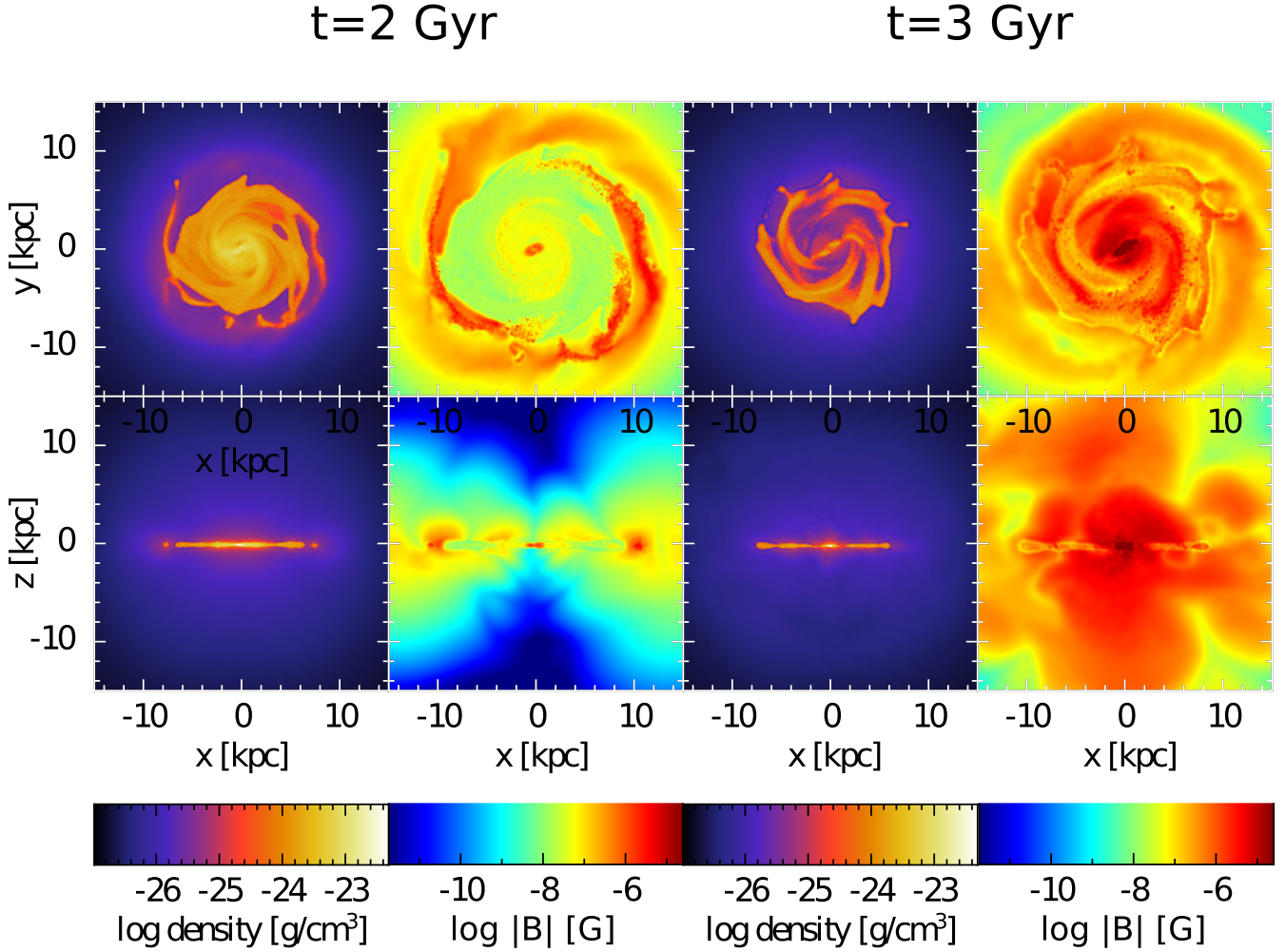


**Figure 2.** Projected gas densities (first and third row) and projected magnetic field strengths (second and fourth row) for the model *MW-SnB* for two different points in time. The four panels on the left show the galaxy at  $t = 2$  Gyr and the four panels on the right show the galaxy at  $t = 3$  Gyr. For  $t = 2$  Gyr, the thermal pressure is the dominating component in the ISM. The gas is captured in the potential minimum and forms a razor thin disc. For  $t = 3$  Gyr, the situation has changed and the magnetic pressure is dominating the system driving winds with mass-loss rates of the order of a few  $M_{\odot} \text{ yr}^{-1}$ . We find three amplification processes at work in this kind of simulation. In the beginning, the magnetic field is amplified in the centre via adiabatic compression and a small-scale turbulent dynamo in the centre, while in the outer parts the magnetic field is amplified by the  $\alpha-\Omega$  dynamo. At later times, the small-scale turbulent dynamo is ultimately switched off by the strong magnetic fields and only the  $\alpha-\Omega$  dynamo remains.

magnetic field lines start to bend and form a sinusoidal shape around the mid-plane. The mass on top of the field lines starts to flow down as mass can move freely alongside the field lines in direction of the strongest gravitational potential in the centre. This is significantly reducing the mass that confined the magnetic field line against the uprising pressure and the field lines rise. This process continues until the field line reaches the edge of the disc. The density in the ambient CGM is orders of magnitude lower than in the disc. The magnetic pressure drives a wind into the CGM. The outflow velocity is hereby limited by the speed of sound within the CGM which is a few  $100 \text{ km s}^{-1}$ .

In Fig. 4 we show the streamlines of the velocity within  $10 \text{ kpc}$  for two different points in time,  $t = 2$  Gyr (left) and  $t = 2.5$  Gyr (right) in the face-on view (top) and the edge-on view (bottom). The face-on velocity structure is very regular. The gas is orbiting the centre of the galaxies in circular orbits before the outflow sets in. In vertical direction, the centre of the galaxy is accumulating

mass from the CGM, which gravitationally destabilizes the central region and leads to the formation of a bar in the innermost  $\text{kpc}$  of the disc. To obtain a more detailed insight in the velocity structure, we show the three-dimensional velocity structure for four different points in time before (top left) during peak outflow (top right), in transition to a decaying outflow (bottom left) and past the outflow (bottom right) in Fig. 6. The darker colour shows higher velocities. We can see that the regular rotating velocity structure is disturbed by the outflowing material that eventually falls back to the disc. After this material settles again and the outflow stops, the disc circular motion is dominating the system again. In Fig. 5, we show the same streamline maps as in Fig. 4 but for the magnetic field lines. Adiabatic compression amplifies the magnetic field, the magnetic pressure rises, and magnetic field lines are pushed towards the CGM on the time-scales of roughly  $500 \text{ Myr}$  in good agreement with the time-scale of the Parker instability. We find that the magnetic field structure is highly complicated due to the ongoing dynamo action in the disc. This is present before and after the outflow sets in. Once

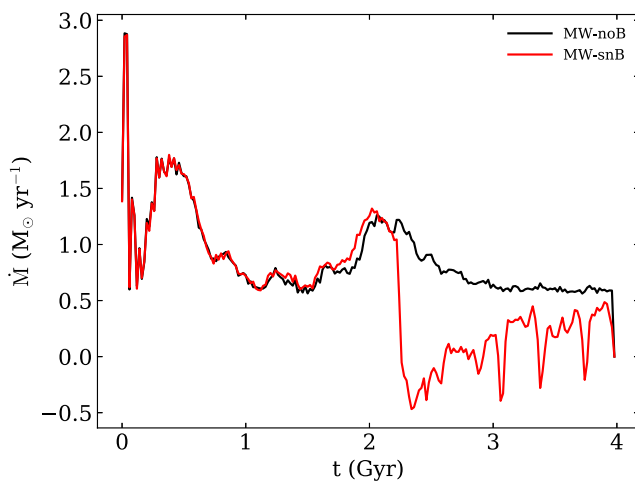


**Figure 3.** We show the mass budget of the models MW-snB that utilizes magnetic seed fields via the seeding of SNe compared to the model MW-noB that represents an fluid with infinite plasma  $\beta$  (hydro-dynamic limit). We clearly see that the mass budget of the simulation without magnetic field stays positive all the time due to smooth accretion from the hot CGM (black line). The simulation with magnetic field is also smoothly accreting material. However at roughly 2.3 Gyr we see a drop with a peak outflow rate of 0.5 solar masses per year. While this outflow is small compared to mass loadings of SN feedback or even AGN feedback, it is capable not only to prevent the smooth accretion from the CGM, but also to remove star-forming gas from the galactic disc.

the field lines reach the edge of the disc they expand freely into the CGM until they reach the speed of sound where the pressure support becomes weak and the outflow velocity saturates. The wind itself is then driven by uprising magnetic field lines due to the Parker instability and can be imagined as a magnetic supper bubble of Parker-lobes forming in the centre and rising to the edge of the disc where they finally breakup and expand towards the CGM (bottom right of Fig. 5). This can be seen even more clear in the corresponding three-dimensional streamline maps of the magnetic field that we show in Fig. 7 for the same points in time at which we determined the three-dimensional velocity maps from Fig. 6. While the magnetic field structure only builds up in the disc in the beginning due to the fact that the dynamo action is restricted to the disc (top left of Fig. 7) at later times we can observe Parker-like bending of the magnetic field lines which supports our proposed outflow mechanism (top right panel of Fig. 7). Once the outflow starts to decay these Parker-like lobes start to get twisted while they are falling back (see bottom left of Fig. 7) to the disc generating the highly complicated magnetic field structure after the outflow settles (bottom right of Fig. 7). Moreover we note, that the direction of the outflow by this mechanism can be determined a priori. The field lines within the disc basically see the same density contrast in the  $xy$ -plane. However, in the  $xz$ -plane, the field lines see the highest density contrast which leads to the highest pressure gradient which makes the Parker instability very effective in the  $z$ -direction in our simulations while it is suppressed in the disc by the relatively constant pressure background.

#### 4.2 Structure of the outflow

We briefly discuss the structure of the magnetic driven outflow. In Fig. 8, we show the distribution of the densities within the outflow.

The distribution peaks at a number density of around  $0.003 \text{ cm}^{-3}$  leading to the conclusion that most of the gas in the outflow is very low density gas which is not star forming. This is in agreement with the picture of the Parker instability as the driver for the outflow. The mass on top of the field lines that bend due to the Parker instability is falling down along the field lines reducing the mass that supports the line against the uprising magnetic pressure. The top of the field line consists therefore of lower density gas that is pushed out by the pressure. This becomes even more clear by considering the bottom panel of Fig. 8 in which we show a temperature–density phase-space diagram. We can clearly identify the galactic disc as the branch that is at high densities and low temperatures. Vice versa we can see the CGM clearly at low densities and high temperatures. The structure between those two components can be explained by considering cooling from the CGM to the disc and outflowing gas from the disc to the CGM. The outflowing gas is hereby the low-density gas branch of the connection between CGM and disc, while the cooling gas is feeding the centre of the galaxy toward higher densities. This finally leads to a bar-instability that initiates the outflow process. The gas is then first adiabatically expanded and cools before it is lifted above the disc where it is heated by the hot halo gas, stabilizing the complicated baryon cycle between the disc and the CGM.

Further, we investigate the outflow velocities. In Fig. 9, we show the structure of the outflowing velocities for four different points in time, before the outflow (upper left), at the beginning of the outflow (upper right), during the outflow (lower left), and at a later stage where the outflow gets weaker again. Before the outflow sets in we find a very narrow distribution of the velocities perpendicular to the disc with velocities of a few  $\text{km s}^{-1}$ . When the outflow starts we find a very wide distribution of velocities that reaches out to roughly  $600 \text{ km s}^{-1}$ . The peak in the centre are the particles that belong to the disc. At a later stage of the outflow, most of the particles are flowing out with velocities between  $50 \text{ km s}^{-1}$  and  $250 \text{ km s}^{-1}$  with an extended tail of particles that can reach still velocities up to  $600 \text{ km s}^{-1}$ . We note that these particles are located in the outer regions of the CGM. At late stages the outflow gets weaker due to the declining gas mass fractions as a result of star formation and the outflow itself. As the outflow-velocities are smaller than the escape velocity, the majority of the particles falls back to the disc on the time-scales of a few 100 Myrs. This recycling flow can be seen in the bottom right panel of Fig. 4.

## 5 GALACTIC DYNAMO IN MW-LIKE GALAXIES

### 5.1 Structure of the magnetic field

First, we discuss the general magnetic field structure. In Fig. 2, we show the projected gas densities and projected magnetic field strengths for two different points in time. We are able to follow three different amplification processes of the magnetic field in this simulation, adiabatic compression of the field lines, the small-scale turbulent dynamo (on time-scales of a few tens of Myrs) and the  $\alpha$ – $\Omega$  dynamo (on Gyr time-scales). In the beginning of the simulation, the magnetic field is amplified in the outer parts due to large-scale rotation and in the centre through amplification via turbulence induced by the feedback of SNe. Later, the formation of the bar in the centre leads to an increase of the magnetic field strength due to adiabatic compression. Material can effectively be transported to the centre due to the bar following the radial field lines within

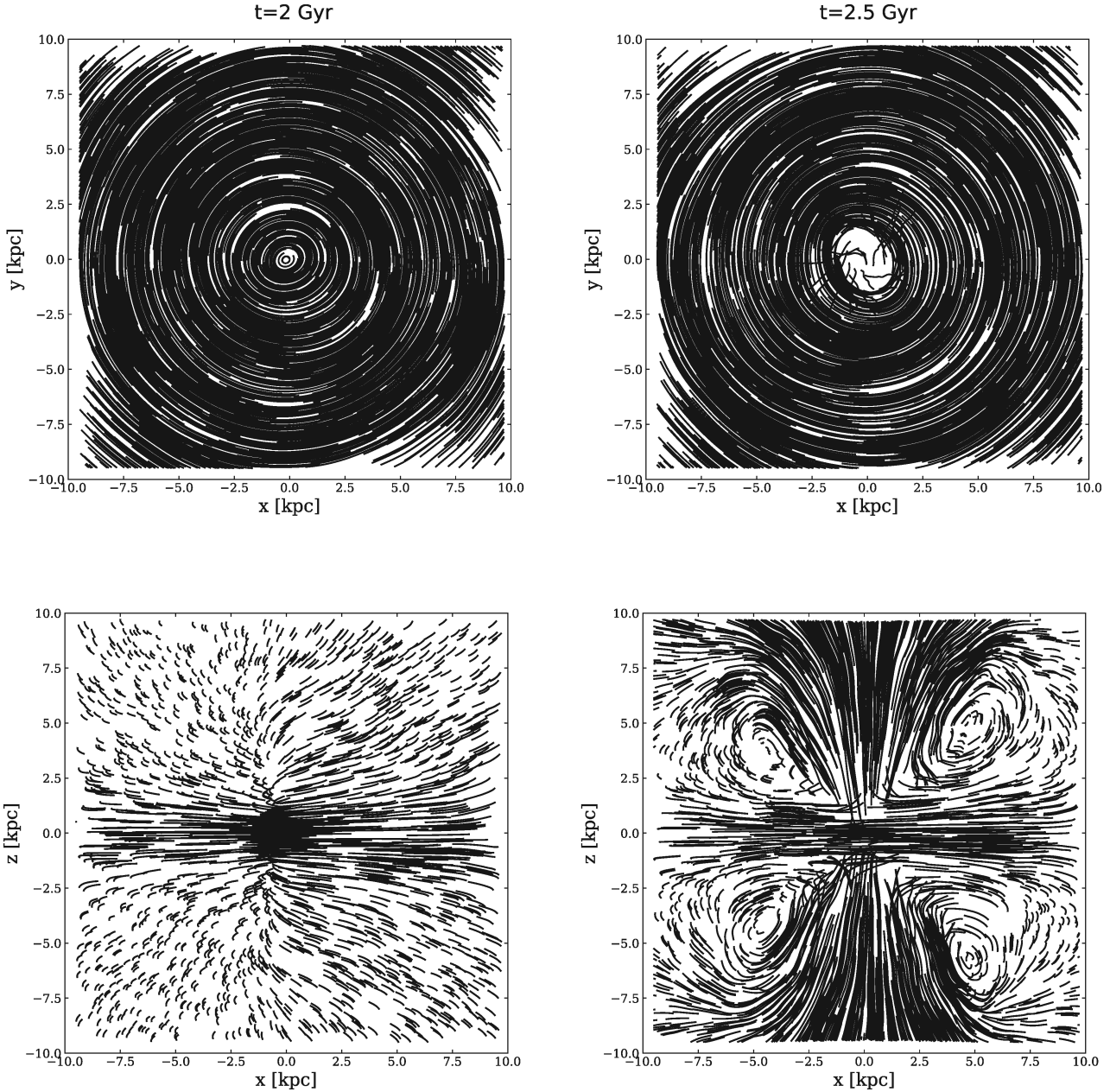


**Figure 4.** Structure of the velocity field for  $t = 2$  Gyr on the left face-on (top) and edge-on (bottom) and for  $t = 2.5$  Gyr on the right. The gas within the disc rotates differentially until the outflow sets in. Shortly, before the outflow sets in we find that there is an inflow from the CGM to the very centre of the galaxy which subsequently increases the density in the centre and adiabatic compression leads to an increase of the magnetic pressure that subsequently drives the outflows. When the outflow is present we see that the gas is moving in  $z$ -direction and falls back at later times.

the bar. The Parker instability determines the threshold for increase of the magnetic field within the disc until the field lines break out of the disc and form two giant magnetized lobes that lead to the magnetic outflow. In Fig. 10, we show the total magnetic field as a function of the radius and compare to the observations of Beck (2001) and Berkhuijsen et al. (2016). We show the total magnetic field at the end of the simulation and excluded the star-forming gas from the calculation to have the closest comparison possible to the observations at hand. We note that we find values that are a factor of 2.5 too low compared to these observations. However, we do not follow the disc's cosmological evolution and thus we do not expect the disc to have a fully developed field in the outer parts of the

galaxy. Moreover, the disc is accreting gas from the halo which is not enriched with magnetic field yet. This can substantially reduce the disc's magnetic field in the outer parts compared to galactic models that do not exclude a hot CGM and can easily lead to a factor of a few lower values of the magnetic field in the radial trend. Furthermore, to self-consistently derive the magnetic field strength we would need to generate RM-mock observations to have a closer comparison with observations, which we will focus on in future work. In Fig. 11, we show the radial profiles in the galactic disc for the radial and toroidal components of the magnetic field. In the beginning of the simulation both components appear to be flat as a function of the radius. This is due to the fact that at this point in time

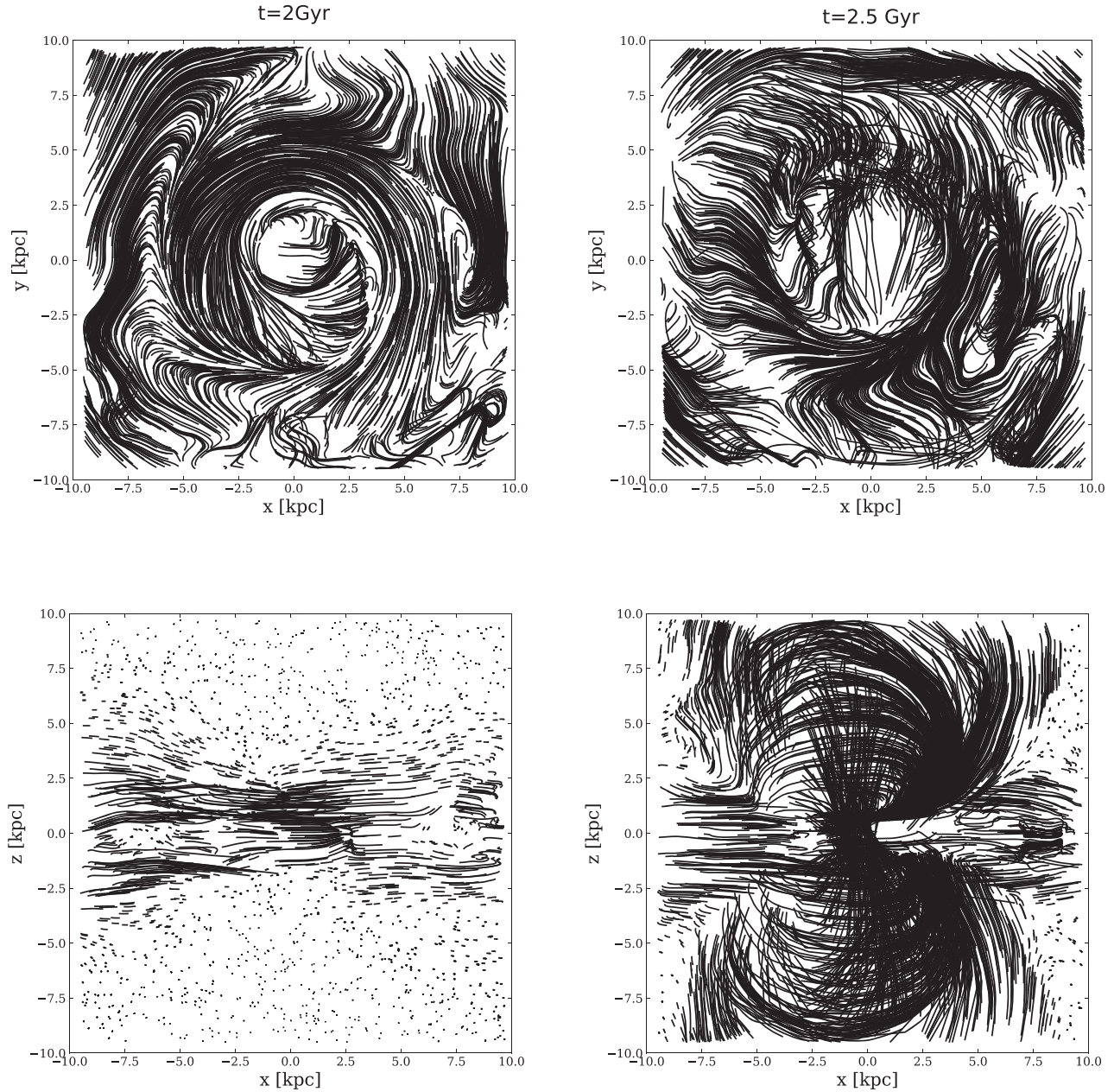


**Figure 5.** Structure of the magnetic field for  $t = 2$  Gyr on the left face-on (top) and edge-on (bottom) and for  $t = 2.5$  Gyr on the right. Already in the beginning of the simulation we find a highly complicated structure in the magnetic field that is kept once the outflow is present at later times. In the  $z$ -direction, we find at later times that the field lines rise and their structure is in good agreement with what is expected from the Parker instability.

only a weak background field is present in the simulation, that is only seeded by the SNe in the ambient ISM due to our SN-seeding mechanism. This small seed fields have to be amplified first. This indicates that there is only weak dynamo action in the first Gyr of the simulation. However, after that point in time we can see that both the radial and the toroidal magnetic field component change its sign as a function of radius. Observationally, this behaviour is correlated with ongoing dynamo action within the galactic disc (Beck 2015; Stein et al. 2019). In a dynamo the toroidal magnetic field component is generated via differential rotation from the radial field. This effect is captured in the appearing asymmetry of the radial and the toroidal magnetic field components.

Moreover, we can investigate the structure of the magnetic field as a function of the height above the mid-plane. We show the results for the radial and toroidal magnetic field component in Fig. 12. We show the radial field as a function of the scale height on the left for six different points in time and the toroidal field as a function of the disc height on the right. We can use both of these quantities to work out the magnetic field structure that is present around the mid-plane. Dynamo theory predicts a dipole structure or a quadrupolar field structure which results in a certain behaviour of the radial and the toroidal component around the mid-plane. If the radial and toroidal components are antisymmetric around the mid-plane this is an indicator for a dipolar structure of the magnetic field. This

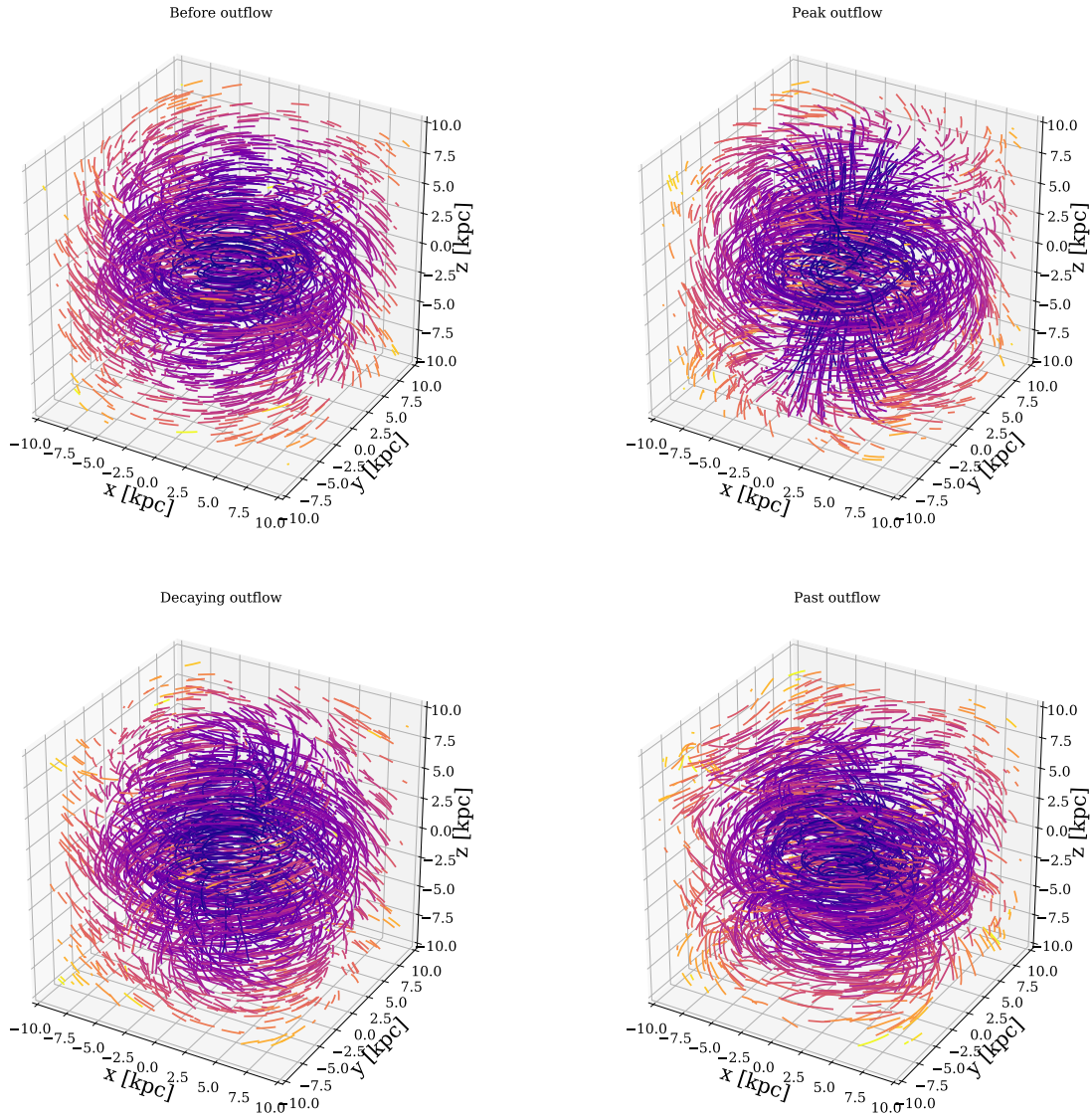


**Figure 6.** Three-dimensional structure of the velocity field at four different points in time, before the outflow (top left), at peak outflow rate (top right), as the outflow decays and the material is falling back to the disc (bottom left) and after the outflow has vanished (bottom right). The colour is indicating the speed of the particles alongside the streamlines, with darker colour showing higher velocities. We can see that once the outflow is emerging the regular velocity structure of the disc that originates from differential rotation is disturbed as the outflow rises with very high velocities from the centre of the disc towards both sides of the CGM. Once the outflow starts to decay the out flowing material falls back to the disc. After the outflow is over the disc relaxes to a more regular rotating state.

picture is consistent with the early stages of the dynamo within our simulations. We find relatively weak magnetic fields in radial and toroidal direction indicating a dipole structure of the magnetic field. However, at later stages the symmetry becomes even which indicates quadrupolar field structure. However, we note that we find an increase of the magnetic field in the mid-plane for both components once the system becomes outflow dominated. Further, we note that we find several field reversals at later stages with an even symmetry which not only predicts a quadrupolar field structure but also predicts a dynamo with several higher modes.

## 5.2 Pitch angle

From observations there are two strong indicators for ongoing dynamo action within a galaxy. The first one is the behaviour of

the radial and toroidal components of the magnetic field, the second one is the pitch angle  $p$  which provides straightforward evidence for dynamo action. This is the shape of the projected magnetic field lines on to the plane of the galactic disc and is given by

$$\tan p = \frac{B_r}{B_\varphi}, \quad (11)$$

where  $B_r$  and  $B_\varphi$  are the radial and toroidal component of the magnetic field given in cylindrical coordinates given by

$$B_r = B_x \sin(\varphi) + B_y \cos(\varphi), \quad (12)$$

$$B_\varphi = -B_x \cos(\varphi) + B_y \sin(\varphi). \quad (13)$$

From observations the pitch angle can be constrained between  $-30$  and  $-10$  deg (e.g. Fletcher et al. 2000) which is in good agreement

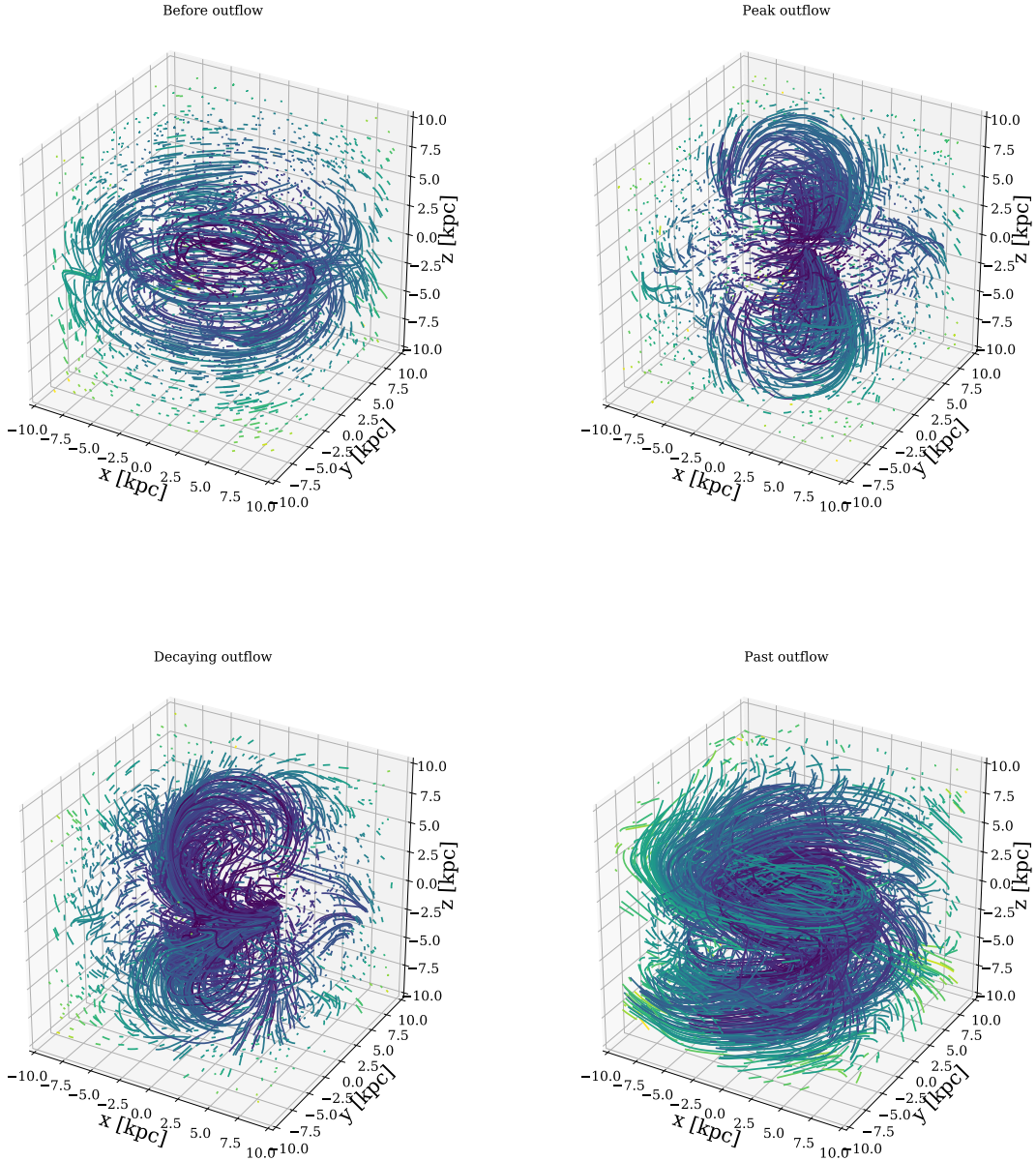


**Figure 7.** Three-dimensional structure of the magnetic field at four different points in time, before the outflow (top left), at peak outflow rate (top right), as the outflow decays and the material is falling back to the disc (bottom left) and after the outflow has vanished (bottom right). The colour is indicating the strength of the magnetic field with darker colour showing higher magnetic field values. we can see that once the outflow is present we can observe two Parker-like lobes rising above and below the disc. This clearly shows the bending of the magnetic field lines by the Parker instability which is the initial process for the outflow to form. At later times when the material starts to fall back towards the disc we can see that the structured of these lobes is altered which finally results in a highly complicated magnetic field structure once the outflow has vanished.

with our results. We derived the pitch angle from our simulation via equation (11) and show the result for six different points in time in Fig. 13. At early times the pitch angle is negative at a value of around  $-5$  deg and stays roughly constant as a function of the radius. At later times we find pitch angles between  $-30$  (in the centre) and  $-5$  deg (in the outer parts). We note that we find also positive pitch angles due to the structure in the distribution of the magnetic field. At early stages this fluctuations of the magnetic field are mostly due to the noise of our underlying numerical scheme. At later stages, the structure of the magnetic field is mostly introduced by the outflow in the centre which leads to a perturbation of the system. The bump at roughly 12 kpc can be explained by hot gas that is cooling down to the disc and a resulting accretion shock.

Once our system becomes dominated by the outflow in the very centre the spiral structure becomes disrupted in the innermost area of the galactic disc. Therefore, we can see a positive pitch angle in this regime where our trailing spiral arms lifted and twisted by uprising material from the disc that is accelerated by the magnetic pressure. The pitch angle can be estimated directly from dynamo theory in different limits. We find good agreement with the results of Shukurov (2000) who computed the pitch angle via

$$\tan p = -\frac{l}{h} \sqrt{\frac{\Omega/r}{\partial \Omega / \partial r}}, \quad (14)$$

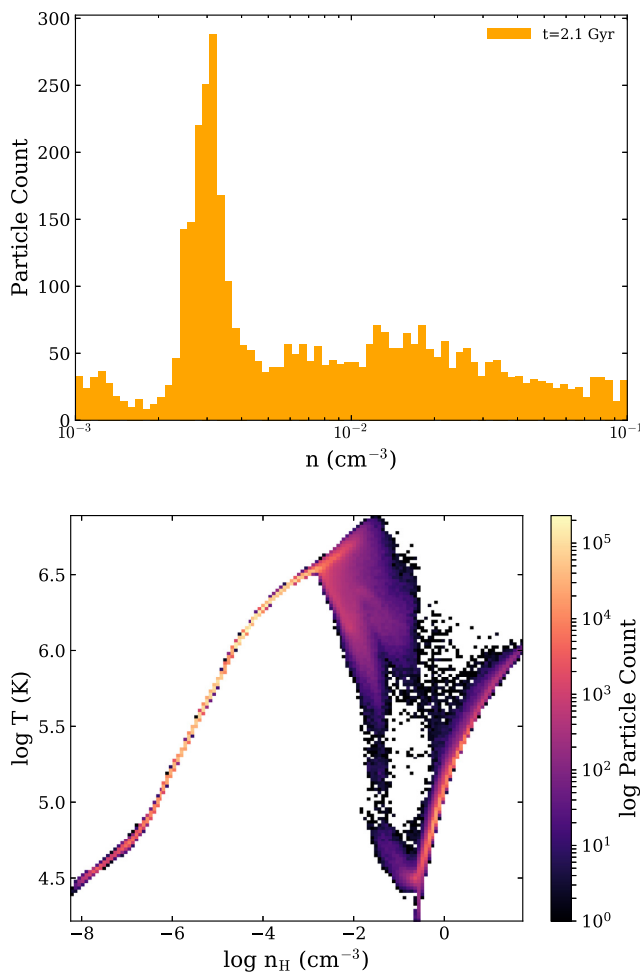


**Figure 8.** **Top:** Density structure of the outflowing gas that is pushed out by the magnetic pressure. The peak number density is around  $0.003 \text{ cm}^{-3}$  which is in good agreement with results from Girichidis et al. (2016) who find a similar peak number density of the outflowing gas. In the case of Girichidis et al. (2016) the outflow is driven by the feedback of SNe. Surprisingly, we find that our outflow which is driven by the magnetic pressure can generate a similarly structured outflow. **Bottom:** Temperature–density phase space diagram. We can easily distinguish between the galactic disc (low temperature and high densities) and the CGM (high temperature and low densities). These two phases interact via cooling from the CGM to the disc and the outflowing gas from the disc to the CGM. Hereby the outflowing gas can be seen as the branch that is walking up from low densities in the disc towards higher temperatures and lower densities to the CGM between  $0.001$  and  $0.01 \text{ cm}^{-3}$ . Thus the gas first cools due to adiabatic expansion (switching off star formation in the process) before it is lifted above the disc and heated by the surrounding medium of the CGM.

with  $l$  as the disc scale length and  $h$  as the disc scale height. For a flat rotation curve, the term in the square root of equation (14) is one and the pitch angle is only dependent on the ratio  $l/h$ . For a Milky Way like galaxy, this gives a pitch angle of roughly  $-15$  deg. However, we note that this limit is only valid if the parameter  $D_{\text{crit}}$  is close to one. A more detailed calculation with a better treatment for  $D_{\text{crit}}$  is presented by Ruzmaikin et al. (1988a). Further, we find agreement of the pitch angle with the results from Moss (1998) and Haud (1981) and note that our structure for the pitch angle is close to the  $\alpha^2 - \Omega$  dynamo shown in Moss (1998). This is especially true in the outer parts of the disc which we show as the thick black solid line in Fig. 13. Moreover, we over plotted the observational results

of Fletcher et al. (2000) for the Andromeda galaxy as the magenta triangles.

### 5.3 Dynamo control parameters

We determine the so-called dynamo control parameters. In the literature, there are two Dynamo parameters of interest that measure the contribution of the  $\alpha$ -effect ( $R_\alpha$ ) and the contribution of the  $\Omega$ -effect ( $R_\omega$ ). They are given by

$$R_\alpha = \frac{\alpha h}{\beta}, \quad (15)$$

$$R_\omega = \frac{G h^2}{\beta}, \quad (16)$$

where  $\alpha$  is the strength of small-scale vertical flows given by  $\alpha = l^2 \Omega / h$  with the turbulent length-scale  $l$ , the angular velocity  $\Omega$ , and  $h$  is the scale height of the disc.  $G = r \partial \Omega / \partial r$  is the shear rate that we can directly obtain from the shape of the rotation curve of our Milky Way like galaxy. The factor  $\beta = 1/3 l v_{\text{turb}}$  with the turbulent length-scale  $l$  and the turbulent velocity  $v_{\text{turb}}$ .  $R_\alpha$  and  $R_\omega$  define the dynamo number  $D = R_\alpha R_\omega$  which indicates Dynamo action for  $|D| > |D_{\text{crit}}|$ , with  $|D_{\text{crit}}| \approx 10$ . Before we start the determination of the dynamo control parameters, we justify the assumptions under which we choose some of the parameters from above to actually determine the dynamo control parameters. Especially, we want to justify our choices regarding the turbulent length-scale  $l$  and the turbulent velocity  $v_{\text{turb}}$  that we assume for our simulated galaxy. First, we note that within our galactic model it is hard to track turbulence in the first place which is due to our pressure floor sub grid model. However, keeping this issue in mind, determining the turbulent length scale can be self-consistently done by computing the velocity power spectra and measuring the injection scale for our induced turbulence before the start of the turbulent cascade. We obtain the power spectra with the code SPHMAPPER (Röttgers & Arth 2018) by properly binning the data to a mesh with the same kernel that we used for our SPMHD simulation. By doing this, we obtain an injection scale of roughly 100 pc. This value is in very good agreement with the radius of SN remnants at the time of pressure equilibrium (e.g. Kim & Ostriker 2015). For the turbulent velocity, we assume the mean rms of the velocities in each bin. For most bins, this value is roughly around  $10 \text{ km s}^{-1}$ . We show radial profiles of the our rotation curve (top left), and the dynamo control parameters  $R_\alpha$  (top right) and  $R_\omega$  (bottom left) and  $D$  (bottom right) for six different points in time in Fig. 14. We note that the shape of the dynamo control parameters is very similar between  $R_\alpha$ ,  $R_\omega$ , and  $D$  but the normalization is different. This is mainly driven by the similar shape of the rotation curves and the fact that radial change of the shear goes as  $-\Omega$  (in the leading term). We find radially declining dynamo parameters for all times that we display. Moreover, we note that we plot the absolute value of the dynamo numbers. At early times we find that  $D$  is greater than 10 in the very centre, indicating ongoing dynamo action (e.g. Shukurov et al. 2019). At later times, the dynamo parameters decrease faster and go below 10 in the centre. Although that would indicate that dynamo action is suppressed, we note that the launching outflow introduces a lot of noise within our bins for the turbulent velocity as we measure it as the velocities  $z$ -component. Therefore, we overestimate the turbulent velocity in the central bins by at least a factor of 2 which would then lead to dynamo control parameters larger than 10 showing still ongoing dynamo action in the presence of the outflow.

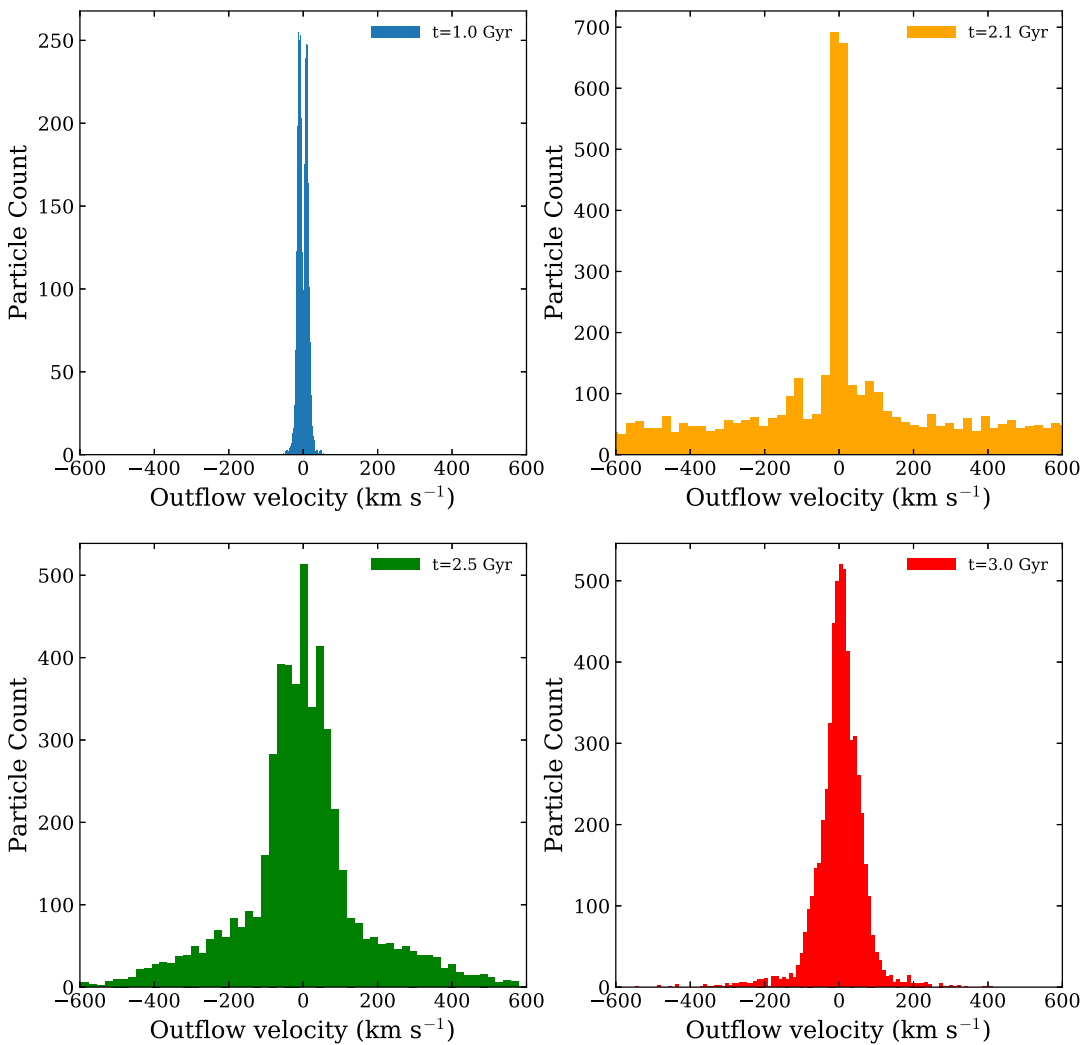


**Figure 9.** Histograms of the outflowing gas for four different points in time at  $t = 1$  Gyr before the magnetic driven outflow sets in (top left), at  $t = 2.1$  Gyr shortly after the onset of the outflow (top right), at  $t = 2.5$  Gyr during the outflow (bottom left) and at  $t = 3$  Gyr (bottom right) when the outflow becomes weaker again. We only investigate the star-forming gas that is evacuated from the disc. This process reduces SFR and magnetizes the CGM. The high outflow velocities are in good agreement with the upper limit for a pressure driven wind, set by the sound speed within the CGM. Further, we note that the magnetic pressure of the galactic magnetic field drives the outflow. The field lines rise due to the Parker instability until they break out of the galactic mid-plane. Then they are pushed forward by the magnetic pressure from the galactic centre.

## 6 CORRELATION BETWEEN STAR FORMATION RATE AND MAGNETIC FIELD

We investigate the dependence of the magnetic field on the SFR. Schleicher & Beck (2013) find that the magnetic field scales with the SFR in the following manner:

$$B \propto \Sigma_{\text{SFR}}^{1/3}. \quad (17)$$

In Fig. 15 we show that the star formation is following the Kennicutt relation for four different points in time. This fact has an direct impact on the correlation of the SFR with the magnetic field. This is shown in Fig. 16 where we show the dependence of the magnetic field and the SFR surface density  $\Sigma_{\text{SFR}}$  for four different points in time,  $t = 1.5$  Gyr (top left),  $t = 2.0$  Gyr (top right),  $t = 2.5$  Gyr (bottom left), and  $t = 3.0$  Gyr (bottom right). The orange and the magenta solid lines show the power law dependencies that can be obtained from observations in the neutral and the molecular

regime. The red dots are obtained by binning the whole galaxy on a grid with  $256 \times 256$  cells. The magnetic field is then obtained by integrating the LOS magnetic field. The star formation surface density is obtained by integrating the LOS SFR and normalizing it by the unit area. Therefore, we can follow the global dependence of the SFR surface density and the LOS magnetic field. Globally, we find very good agreement with the results of Schleicher & Beck (2013) and observations from Tabatabaei et al. (2013) and Niklas & Beck (1997). However, we note that in a global picture of our Milky Way like galaxy, we are constrained to this behaviour because our star formation is constrained by the Kennicutt relation with a slope of 1.4 for neutral gas and a slope of 1 for molecular gas. For a saturated dynamo where amplification of the magnetic flux can only be obtained by adiabatic compression of the field lines this leads directly to a relation with a similar slope than obtained by Schleicher & Beck (2013). In dwarf irregulars smaller values are obtained (Chyžík et al. 2011), but we find good agreement with

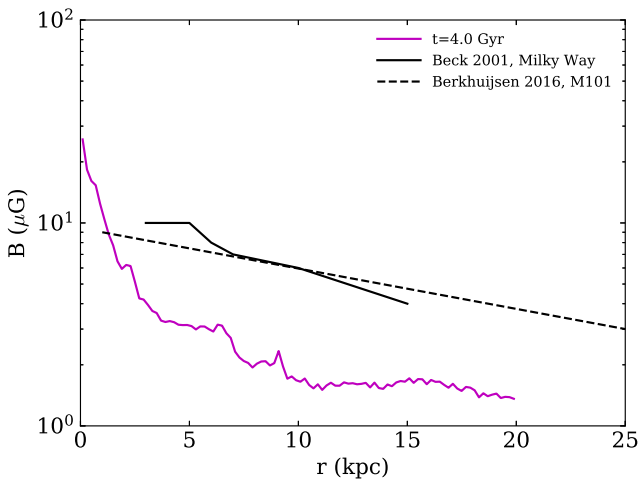


**Figure 10.** Radial profile of the total magnetic field for our final simulation time (magenta). The black solid and the black dashed lines show observations from Beck (2001) and Berkhuijsen et al. (2016) for the Milky Way and M101. We calculated the square root of the mean magnetic field components and excluded the star forming gas to have a consistent comparison with observations. We note that for a better comparison we should construct the RM signal and calculate the total magnetic field from this RM signal. Generally, we find that our simulation predicts a total radial magnetic field that is too low by a factor of 2.5. However, the scatter in both our simulations and the observations is within this range and we capture the declining radial trend.

observations of Milky Way like spirals (e.g. Niklas & Beck 1997). Further, we note the results of Tabatabaei et al. (2018) who observed the centre of NGC 1097 and found an antic correlation between the magnetic field strength and the SFR surface density. We find the same if we look on more local regions of the galaxy. While globally we are constrained by the Schmidt–Kennicutt relation, locally we can find that the magnetic field can behave differently. We show evidence for this behaviour in Fig. 17. Here we plot the magnetic field as a function of the SFR. This gives us the local dependence of

the magnetic field and the SFR. We find regions within the galaxy that do not follow the global power law scaling and the magnetic field is decreasing as a function of the SFR. This is consistent with the findings of Tabatabaei et al. (2018) who observed several molecular clouds in the nearby galaxy NGC 1097 and find a power law scaling with a negative exponent. In our simulations this effect is due to the effect that we include a diffusion term within our induction equation. Magnetic field lines can be transported from the spiral arms to the inter arm regions where they can be twisted and folded by small scale turbulent motion and due to the slightly lower densities but higher temperatures in the spiral arms and subsequently be amplified. Although our resolution is not high enough to properly follow the formation of molecular clouds within the Milky Way ISM, we propose that a similar effect could be responsible for the observed anticorrelation between magnetic field and the SFR in molecular clouds where the magnetic field can be transported and dissipated away from star-forming regions due to non-linear MHD effects and a smaller magnetic field remains in regions with high star formation activity.

## 7 CONCLUSIONS

### 7.1 Summary

We investigated the build-up of the galactic dynamo in a high-resolution simulation of a Milky Way like disc galaxy. We find that the galactic dynamo is supported by the small-scale buoyant bubbles that rise and are twisted by the large-scale rotation of the disc. Further, the dynamo is supported by SN-induced turbulence. Due to the amplification of the magnetic field in the dynamo, the magnetic pressure in the disc quickly amplifies. In combination with the formation of a bar at 1.8 Myr this generates a large-scale galactic outflow that is driven by the magnetic pressure. Further, we investigated the magnetic fields morphology in more detail and computed the pitch angle and the dynamo numbers. In the following, we summarize our most important results.

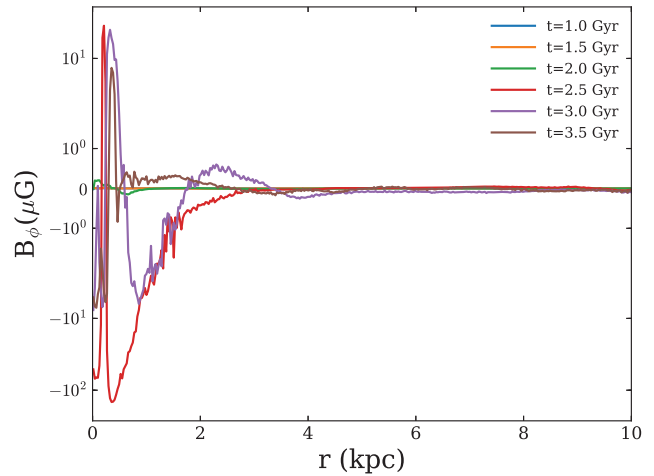
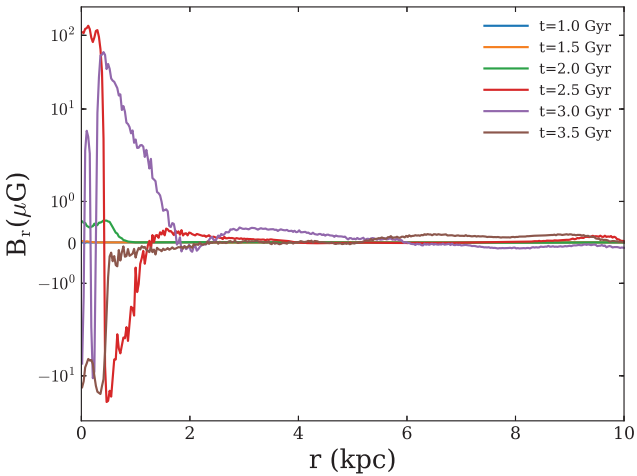


**Figure 11.** Radial profiles in the disc of the radial (top) and toroidal components (bottom) of the magnetic field for the simulation *MW-SnB*, for six different points in time,  $t = 1$  Gyr (blue),  $t = 1.5$  Gyr (orange),  $t = 2$  Gyr (green),  $t = 2.5$  Gyr (red),  $t = 3$  Gyr (purple), and  $t = 3.5$  Gyr (brown). The highest magnetic field strengths can be observed in the centre. Both radial profiles indicate ongoing dynamo action at later stages. In the beginning there is only a weak background field present which is only weakly amplified within the first Gyr. The field is seeded by SNe in the ambient ISM where it is amplified due to small-scale turbulence and large-scale rotation. At later stages the radial magnetic field components change the sign several times as function of the radius. From observations this is known as a first indicator for ongoing dynamo action (Stein et al. 2019).

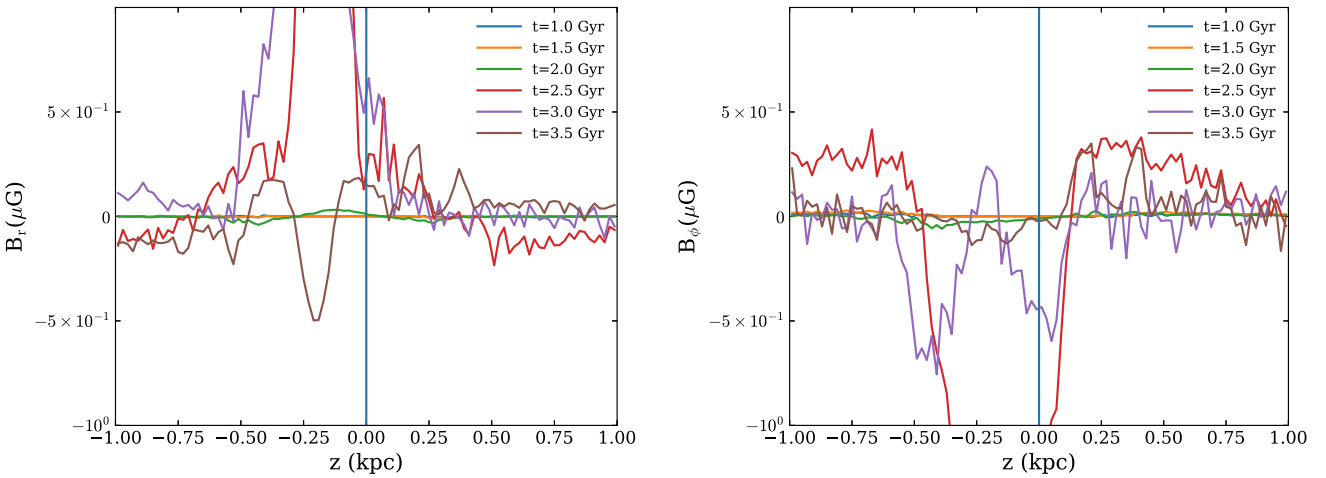


**Figure 12.** We show the dependence of the radial and the toroidal magnetic field component as a function of the disc scale height for six different points in time,  $t = 1$  Gyr (blue),  $t = 1.5$  Gyr (orange),  $t = 2$  Gyr (green),  $t = 2.5$  Gyr (red),  $t = 3$  Gyr (purple), and  $t = 3.5$  Gyr (brown). At early times, we find that the magnetic field distribution is antisymmetric around the mid-plane. This indicates a dipole structure of the magnetic field at early stages of the dynamo. At later stages, we find an even symmetry in the outer part of the galaxy which is indicating a quadrupole field structure. However, we note that at this point the galaxy has build up a wind that is disturbing the magnetic field structure. We find indicators for dipole and quadrupole structure as well in the distribution of the toroidal field. The vertical blue line indicates the position of the mid-plane.

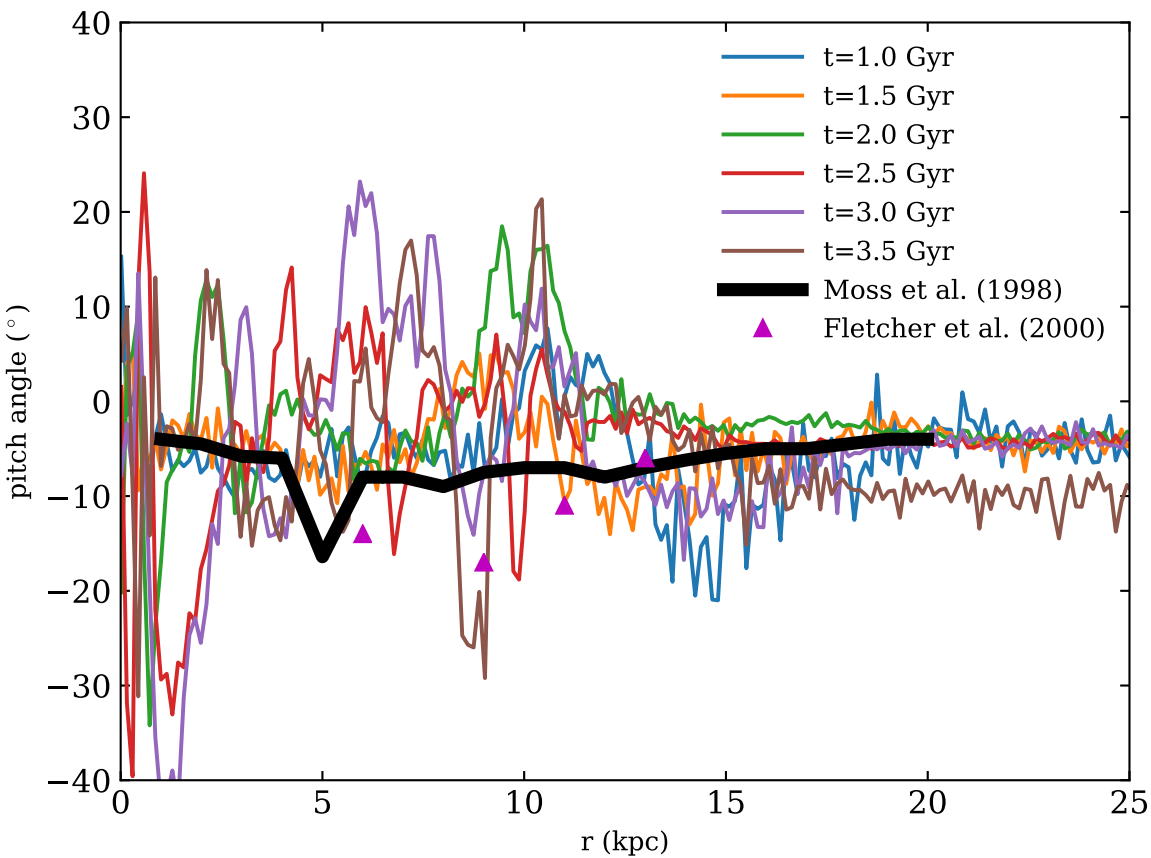


**Figure 13.** Pitch angle as the function of the radius for different points in time,  $t = 1$  Gyr (blue),  $t = 1.5$  Gyr (orange),  $t = 2$  Gyr (green),  $t = 2.5$  Gyr (red),  $t = 3$  Gyr (purple), and  $t = 3.5$  Gyr (brown). At early times before the system is dominated by the outflow in the very centre, we can see negative values for the pitch angle ranging from  $-30$  deg to roughly  $-5$  deg. At later times, we find positive pitch angles because the systems is heavily perturbed by the magnetic pressure driven wind. However, on average we can still reproduce the correct radial trend. This agrees very well with the observations of M31 presented in Fletcher et al. (2000). Moreover, we find a saturation value of roughly  $-5$  deg in the outer parts of the disc which is in good agreement with dynamo models Haud (1981). We find very good agreement with the dynamo model from Moss (1998) who predict an  $\alpha^2 - \Omega$  dynamo. Further, we find good agreement with the Milky Way value which is around  $-15$  deg at the solar orbit of roughly 8 kpc.

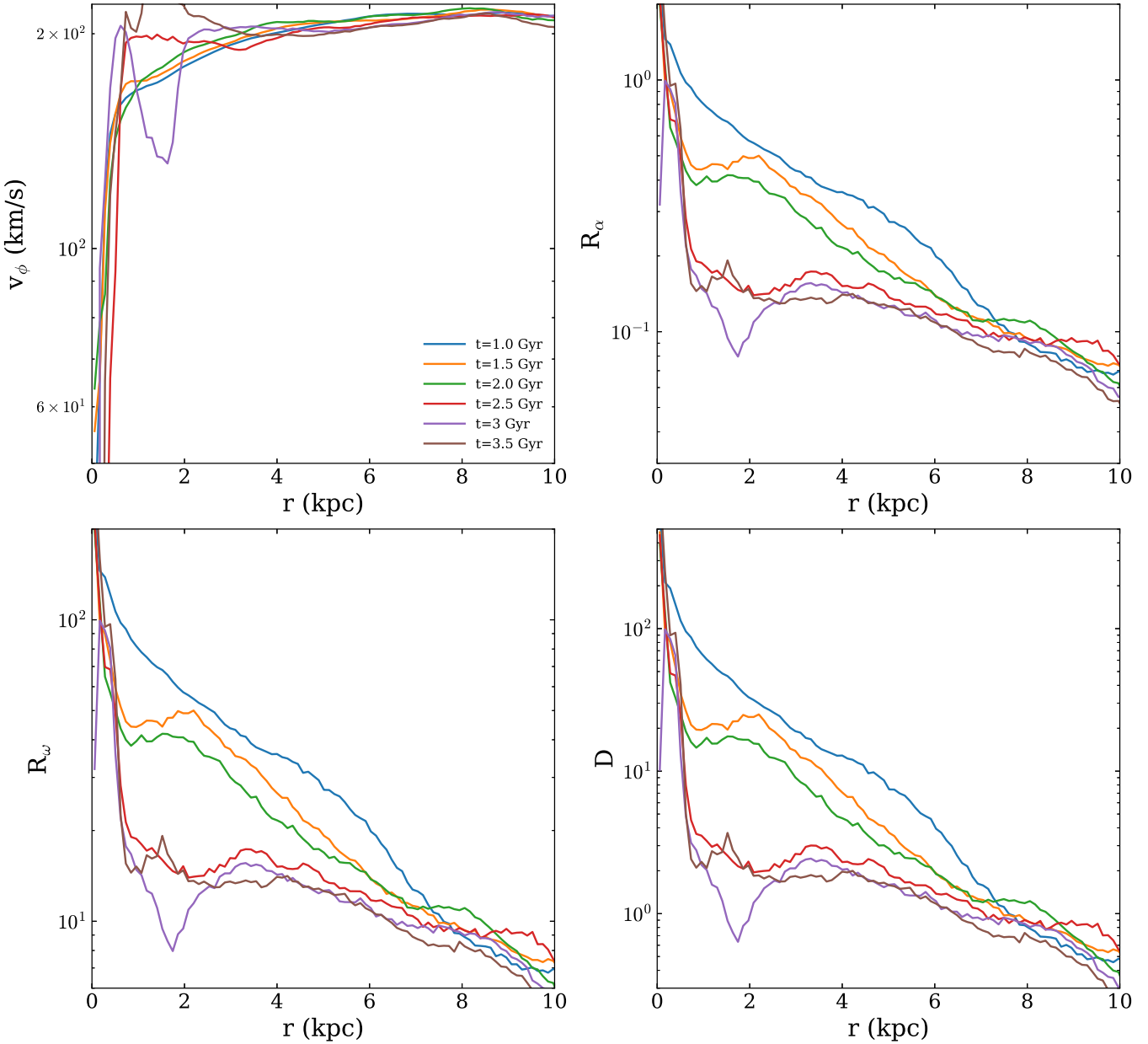


**Figure 14.** Physical properties that are important to classify the galactic dynamo of the galaxy MW-snB for six different points in time,  $t = 1$  Gyr (blue),  $t = 1.5$  Gyr (orange),  $t = 2$  Gyr (green),  $t = 2.5$  Gyr (red),  $t = 3$  Gyr (purple), and  $t = 3.5$  Gyr (brown). The first two points in time are before the outflow sets in, the third point in time is after the outflow is present. **Top left:** Rotation curve of the galaxy as a function of the radius. The rotation curve shows the typical behaviour of a Milky Way like disc galaxy with a steep increase in the innermost 3 kpc and a saturation at around  $200 \text{ km s}^{-1}$  in its outer parts. The oscillation at small radii at later times is a result of the formation process of the bar in the very centre. **Top right:**  $R_\alpha$  as a function of the radius. This parameter quantifies the contribution of the small-scale vertical motion ( $\alpha$ -effect) that is either introduced by small-scale turbulence or rising buoyant bubbles in the inner parts of the galaxy. It decreases with radius as there is only weak feedback present and the gas is mostly in pressure equilibrium. **Bottom left:**  $R_\omega$  as a function of the radius. This parameter quantifies the contribution of the large-scale rotation of the galactic disc ( $\Omega$  effect) to the dynamo process. **Bottom right:** Dynamo number  $D$  as a function of the radius. If the dynamo number is larger than 10 a large-scale galactic dynamo is acting. In the beginning of the simulation, we see a strong dynamo acting up to 6 kpc. At later times when the bar starts to form the dynamo is suppressed and magnetic fields in the centre become amplified via adiabatic compression until the mass inflow to the centre becomes only possible alongside the magnetic field lines due to the rising magnetic pressure.

(i) *Magnetic driven outflows:* We find a magnetic driven outflow driven by the magnetic pressure. Due to the formation of a bar in the galactic centre the mass can be efficiently accreted on to the very centre of the galaxy. The magnetic field is amplified due to adiabatic compression of the field lines which increases the magnetic pressure. On time-scales of a few 100 Myr the field lines in the centre begin to rise due to the buoyancy instability. Once the

field lines reach the edge of the disc, the bubble that is supported by the magnetic pressure can further push out the material at the edge of the disc. The outflow velocity is limited to the speed of sound within the galactic CGM and can reach a few  $100 \text{ km s}^{-1}$ . Although the peak outflow rate is at around  $200 \text{ km s}^{-1}$ , the outflow shows an extended tail towards higher velocities. Therefore, the pressure provided by the magnetic field could indeed play a role for the

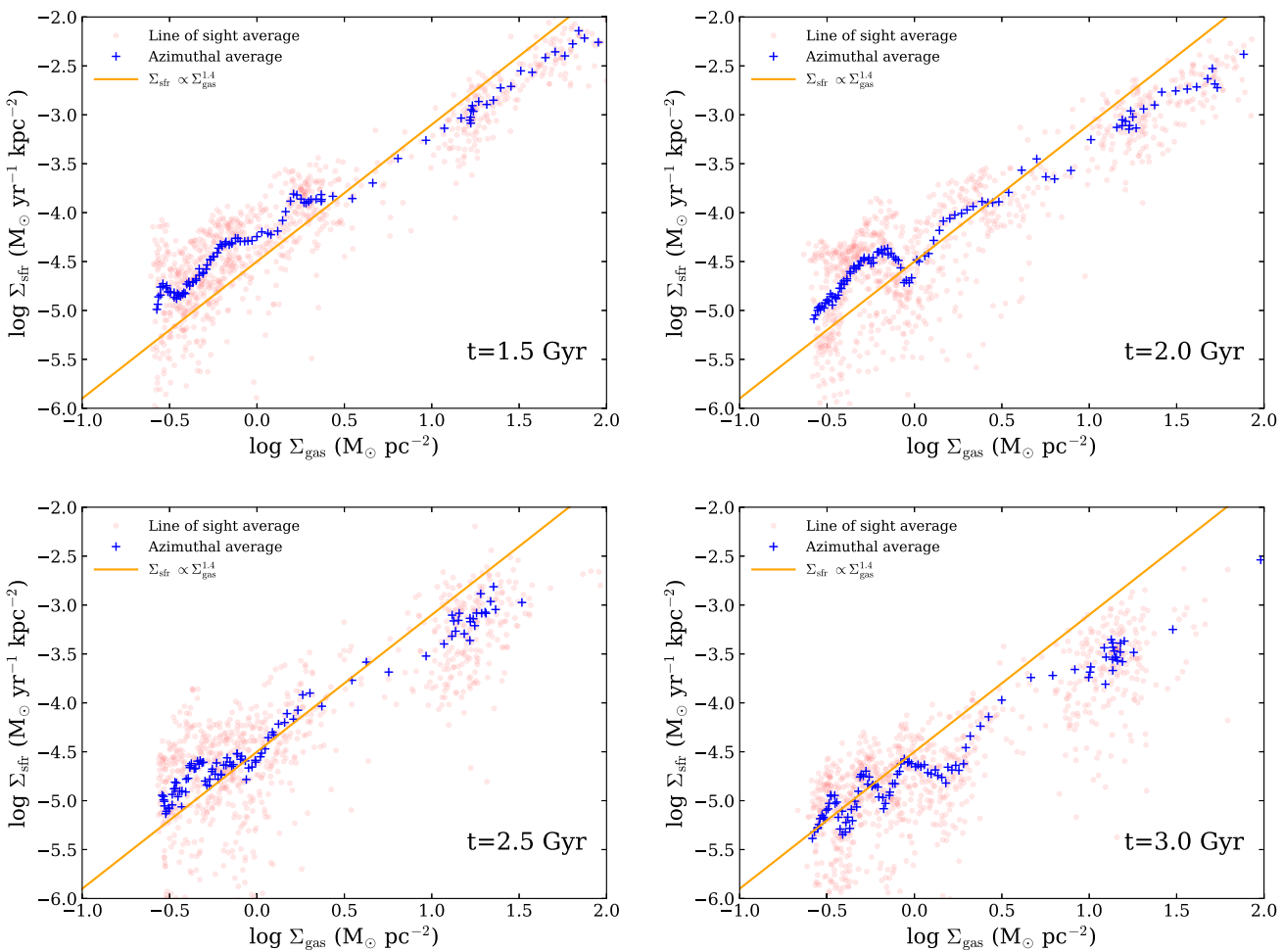


**Figure 15.** SFR surface density as function of the gas surface density for four different points in time,  $t = 1.5$  Gyr (top left),  $t = 2.0$  Gyr (top right),  $t = 2.5$  Gyr (bottom left), and  $t = 3.0$  Gyr (bottom right). The data were obtained by binning the data on a grid with  $256 \times 256$  bins. For every bin, we calculated gas surface density and the SFR density per pixel (red dots). The blue stars indicate the azimuthally averaged values of the red data cloud. In our simulations, star formation follows the Kennicutt relation which we reproduce very good, also at later times within the galaxy.

interpretation of results from Genzel et al. (2014) who observe a similar outflow structure. While they can identify very high outflow velocities with the activity of an AGN the exact origin of the lower velocities remains unclear, but is believed to have SN feedback as an origin.

(ii) *Structure of the magnetic field:* We investigated the detail morphological structure of the magnetic field as function of the radius and disc scale height. In agreement with predictions from dynamo theory we find that field reversals in the radial and toroidal field components. The reversals in the radial component are in agreement with recent observations from Stein et al. (2019) who showed for the first time radial field reversals in observations of the nearby galaxy NGC 4666. Moreover, we find toroidal field reversals which can be observed as well (Beck 2015). Further, we find an indication for an uneven symmetry of the radial magnetic field and the toroidal magnetic field as a function of the disc scale height in the beginning of the simulation. At later times, we find an even symmetry which is especially prominent in the outer parts of the disc. From dynamo theory, it is known that the former is related to a dipole structure of the magnetic field while the latter is indicating a quadrupolar field structure.

(iii) *Pitch-angle:* We investigate the magnetic pitch angle as a function of the radius. Overall, we find good agreement with

our estimated magnetic pitch-angles from our simulations and observations given by Fletcher et al. (2000). Further, we note that our radial trend and the values for the pitch angle are in good agreement with the results of Moss (1998) who find evidence for an  $\alpha^2\Omega$  dynamo which settles in the outer part of the galaxy at roughly  $-5$  deg. We note that we also find positive magnetic pitch angles which do not fit into the picture of the dynamo theory. However, we mostly find them at late times and in the centre of the galactic disc, where the system becomes outflow dominated and the magnetic field structure becomes much more complicated.

(iv) *Dynamo control parameters:* Finally, we compute the dynamo control parameters from our simulation. We measured the turbulent length scale as the injection scale of a velocity power spectrum and calculated the turbulent velocity as the (random) movement of the particles within the disc in  $z$ -direction, by assuming that the motion within the galactic plane is ordered by the large-scale rotation of the disc. From that we obtained dynamo numbers that suggest ongoing dynamo action until the outflow sets in. At later stages the system is outflow dominated and the calculation of the dynamo number becomes more complicated and becomes polluted by particles that belong to the outflow that should not be included in the calculation of the dynamo parameters.

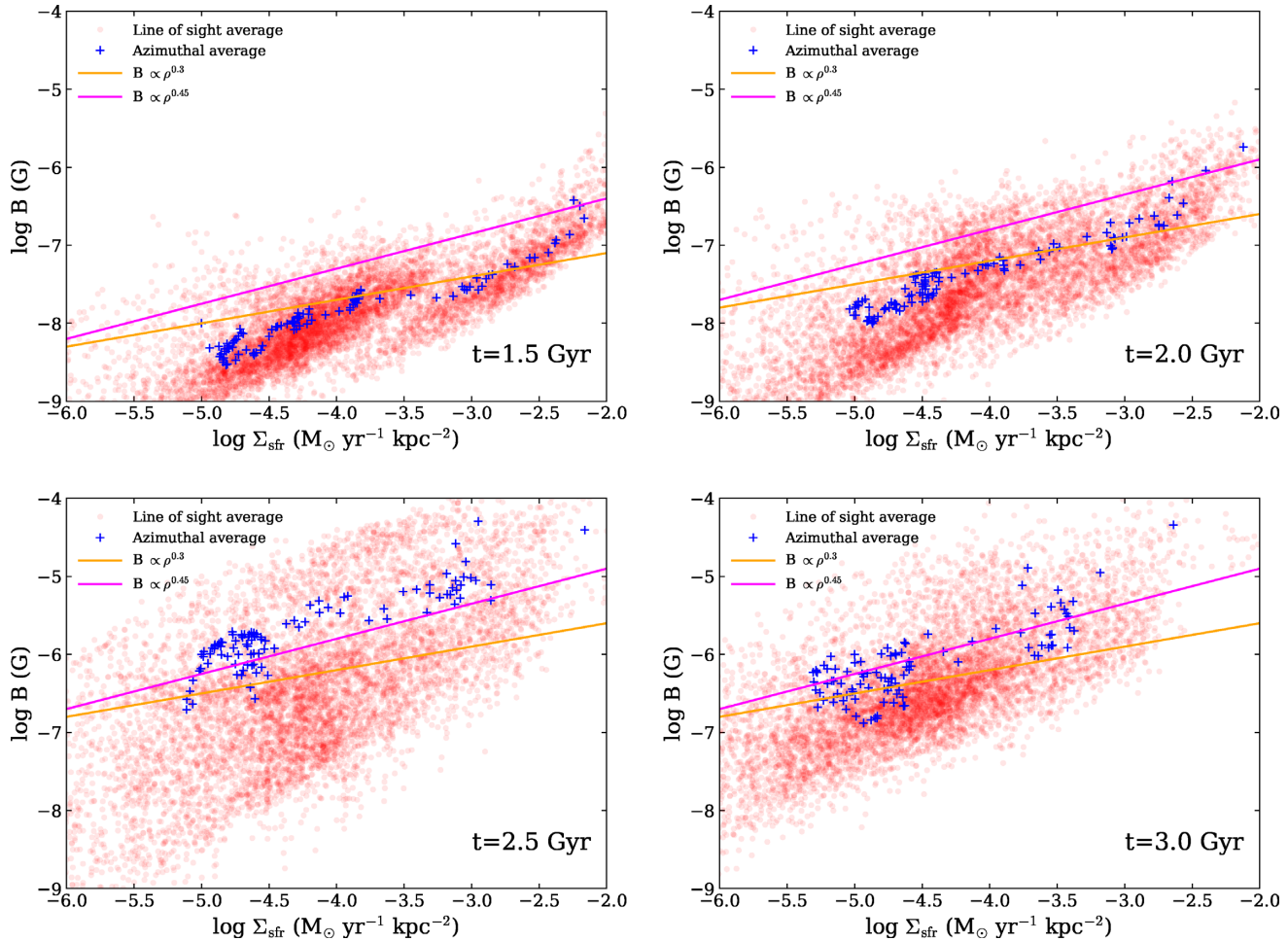


**Figure 16.** Magnetic field as function of the SFR density for four different point in time,  $t = 1.5$  Gyr (top left),  $t = 2.0$  Gyr (top right),  $t = 2.5$  Gyr (bottom left), and  $t = 3.0$  Gyr (bottom right). The data were obtained by binning the data on a grid with  $256 \times 256$  bins. For every bin, we calculated the integrated magnetic field and the SFR density per pixel (red dots). The blue stars indicate the azimuthally averaged values of the red data cloud. The orange solid line shows the relation  $B \propto \Sigma_{\text{SFR}}^{1/3}$  from Schleicher & Beck (2013) which shows good agreement with our azimuthally averaged values. Further, the data we obtain are in good agreement with observations (Beck 2015). The slope of the underlying Kennicutt relation that is affecting the relation between  $B$  and  $\Sigma_{\text{SFR}}$  can vary between 0.3 (for atomic gas, also orange line) and 0.45 (molecular gas, magenta line). However, we note that the scatter in the distribution is relatively large which is a consequence of our stochastic star formation procedure which aims to reproduce the azimuthally averaged Schmidt–Kennicutt relation. Therefore, the agreement with Schleicher & Beck (2013) is a consequence of our star formation law in combination with ideal MHD in the flux freezing regime.

(v) *Relation between SFR and magnetic field:* Globally we find that the SFR scales with the SFR surface density with a power-law slope between 0.3 and 0.45 in good agreement with the results from Niklas & Beck (1997), Schleicher & Beck (2013), and Tabatabaei et al. (2013). However, locally in the spiral arms we find that the SFR can increase while the magnetic field is decreasing due to magnetic dissipation and diffusion which is included in our MHD equations (Tabatabaei et al. 2018).

## 7.2 Model limitations

Although our galactic model works well in reproducing some features known from a galactic dynamo, its predictive power is still limited. First of all, the galactic system is isolated. While this set-up is ideal to gain a deeper understanding of how the galactic dynamo operates it still misses the cosmological background that would be provided by the large-scale structure of the Universe in close proximity of the galaxy. Therefore, we cannot follow the cosmological build-up of the galactic dynamo in a Milky Way

like disc galaxy and the model can by no means be interpreted as a simulation that represents the ab initio generation of a galactic dynamo. As we miss the cosmological framework of the assembly of the Halo via mergers (smooth accretion from the CGM is modelled with the hot Halo) we cannot investigate the influence of major (mass ratio 1:4), minor (up to mass ratio 1:10) and mini mergers (below mass ratio 1:10) on the build-up of the dynamo and the magnetic field evolution of the galaxy. Depending on the type of merger, different scenarios are possible. In the case of minor and mini mergers e.g. Karademir et al. (2019) have shown that the mass of these kind of mergers is mostly deposited in the outer parts of Milky Way like galaxies. Therefore, for these kind of mergers the dynamo properties and the magnetic field evolution is supposedly only weakly influenced. However, major mergers could trigger an overlay starburst of the merging systems (Karademir et al. 2019; Lahén et al. 2019) leading to a significant increase in star formation and turbulence and a more effective amplification of the magnetic field due to the small scale turbulent dynamo and compression of the gas (Steinwandel et al. 2019). This should be investigated in

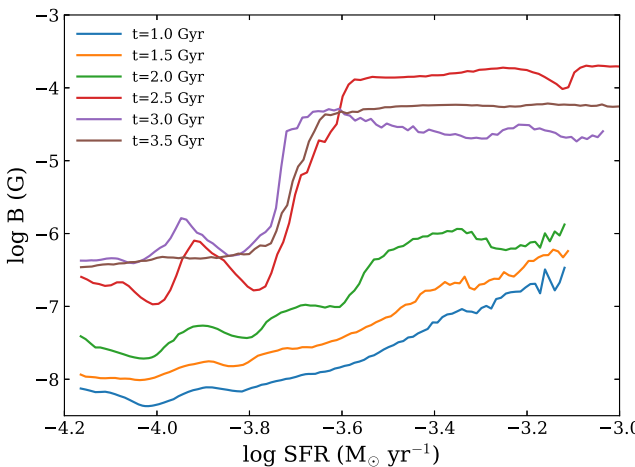


**Figure 17.** Magnetic field as a function of the local SFR for six different points in time,  $t = 1$  Gyr (blue),  $t = 1.5$  Gyr (orange),  $t = 2$  Gyr (green),  $t = 2.5$  Gyr (red),  $t = 3$  Gyr (purple), and  $t = 3.5$  Gyr (brown). At early times, we find that the magnetic field is increasing with SFR. However, at later points magnetic field tends to be constant as a function of the local SFR or is even decreasing. At intermediate time we find that the magnetic field is oscillating with increasing SFR which indicates that there are regions in the galaxy where the local SFR is increasing but the magnetic field is decreasing.

more detail in future studies cosmological zoom-in simulations on galaxy and galaxy cluster scales. However, the consequences for the large-scale  $\alpha\omega$  dynamo that we mainly focused on in this study which orders the field on larger scales are potentially more severe. We note that the small-scale dynamo can amplify the magnetic field on 100 Myr time-scales to the equipartition value (with the turbulent component of the galactic ISM), while the large scale dynamo operates on Gyr time-scales and is more important for re-ordering the magnetic field on larger scales and supporting the field growth once the small scale dynamo saturates. Thus, major mergers can disturb the gas dynamics to a degree that the large-scale dynamo is never fully operating as it is supported by the large-scale disc rotation. This is especially an issue when the merging system consists out of a pro- and counter rotator (miss aligned angular momentum vectors). Another important physics part that is missing within the simulation is the impact of cosmic rays. While the magnetic field alone already has an impact on the evolution of the galaxy the interaction of cosmic rays with magnetic fields is potentially important and has shown to have the capability to drive large scale galactic winds (e.g. Jacob & Pfrommer 2017). Further, we note that we rely on the cooling, star formation, and feedback prescription which is presented in Springel & Hernquist (2003). While this allows us to follow the build-up of interstellar turbulence it mostly remains sub-sonic. Other studies like Su et al. (2018) and Hu (2019) use a more detailed prescription for cooling and feedback that accounts for a proper treatment of momentum generation during the Sedov–Taylor phase of an SN remnant. While this is unlikely to have an effect on the behaviour of the large-scale dynamo, the rapid build-up of supersonic turbulence within the galactic ISM can effect can potentially change the growth rate of the small-scale-turbulent dynamo. Thus, future studies should investigate the build-up of the galactic dynamo with a sub-grid model for cooling, star formation and feedback that accounts for a proper treatment of the small-scale physics of the ISM. Resolving the small-scale structure of the ISM within galaxy formation simulations can therefore help to better

understanding the detailed build-up of the dynamo in Milky Way like galaxies.

## ACKNOWLEDGEMENTS

We thank the anonymous referee for his/her comments on the paper draft, which helped to improve the quality of the paper. We thank Joseph O’Leary, Marcel Lotz, Rhea-Silvia Remus, and Felix Schulze for helpful discussions. UPS thanks Anvar Shukurov and Rashid Sunyaev for useful discussion and insights on dynamo theory and their connection to galaxy dynamics and high-energy astrophysics. UPS acknowledges the discussion with Eugene Churazov, Marat Gilfanov, and Ildar Khabibullin on the details of outflow mechanisms. The authors gratefully acknowledge the computing time granted by the Leibniz Rechenzentrum (LRZ) on SuperMUC under the project number pr86re and SuperMUC-NG under the project number pn72bu as well as the computing time on the c2papp-cluster under the project number pr27mi in Garching where most of this work has been carried out. UPS and BPM are funded by the Deutsche Forschungsgemeinschaft (DFG, German Research Foundation) with the project number MO 2979/1-1. UPS, KD, and AB are supported by the Deutsche Forschungsgemeinschaft (DFG, German Research Foundation) under Germany’s Excellence Strategy – EXC-2094 – 390783311. KD and AB acknowledge support by the DFG Cluster of Excellence ‘Origin and Structure of the Universe’ and its successor ‘ORIGINS’.

## REFERENCES

- Agertz O. et al., 2007, *MNRAS*, 380, 963
- Barnes J., Hut P., 1986, *Nature*, 324, 446
- Basu A., Roy S., 2013, *MNRAS*, 433, 1675
- Beck R., 2001, *Space Sci. Rev.*, 99, 243
- Beck R., 2005, in Wielebinski R., Beck R., eds, Lecture Notes in Physics, Vol. 664, *Cosmic Magnetic Fields*. Springer Verlag, Berlin, p. 41
- Beck R., 2007, *A&A*, 470, 539
- Beck R., 2015, *A&AR*, 24, 4
- Beck A. M., Lesch H., Dolag K., Kotarba H., Geng A., Stasyszyn F. A., 2012, *MNRAS*, 422, 2152
- Beck A. M., Dolag K., Lesch H., Kronberg P. P., 2013, *MNRAS*, 435, 3575
- Beck A. M. et al., 2016, *MNRAS*, 455, 2110
- Berkhuijsen E. M., Urbanik M., Beck R., Han J. L., 2016, *A&A*, 588, A114
- Biermann L., 1950, Z. Nat.forsch. Teil A, 5, 65
- Brandenburg A., 2009, *Plasma Phys. Control. Fusion*, 51, 124043
- Brentjens M. A., de Bruyn A. G., 2005, *A&A*, 441, 1217
- Burn B. J., 1966, *MNRAS*, 133, 67
- Butsky I., Zrake J., Kim J.-h., Yang H.-I., Abel T., 2017, *ApJ*, 843, 113
- Cavaliere A., Fusco-Femiano R., 1978, *A&A*, 70, 677
- Chyžík T., Knapik J., Bomans D. J., Klein U., Beck R., Soida M., Urbanik M., 2003, *A&A*, 405, 513
- Chyžík T., Bomans D. J., Krause M., Beck R., Soida M., Urbanik M., 2007, *A&A*, 462, 933
- Chyžík T., Weżgowiec M., Beck R., Bomans D. J., 2011, *A&A*, 529, A94
- Dedner A., Kemm F., Kröner D., Munz C.-D., Schnitzer T., Wesenberg M., 2002, *J. Comput. Phys.*, 175, 645
- Dolag K., Stasyszyn F., 2009, *MNRAS*, 398, 1678
- Dolag K., Bartelmann M., Lesch H., 1999, *A&A*, 348, 351
- Dolag K., Schindler S., Govoni F., Feretti L., 2001, *A&A*, 378, 777
- Donnert J. M. F., 2014, *MNRAS*, 438, 1971
- Elmegreen B. G., Scalo J., 2004, *ARA&A*, 42, 211
- Fletcher A., 2010, in Kothes R., Landecker T. L., Willis A. G., eds, ASP Conf. Ser. Vol. 438, *The Dynamic Interstellar Medium: A Celebration of the Canadian Galactic Plane Survey*. Astron. Soc. Pac., San Francisco, p. 197

- Fletcher A., Beck R., Berkhuijsen E. M., Shukurov A., 2000, in Berkhuijsen E. M., Beck R., Walterbos R. A. M., eds, Proceedings 232. WE-Heraeus Seminar, p. 201
- Geng A., Kotarba H., Bürzle F., Dolag K., Stasyszyn F., Beck A., Nielaba P., 2012a, *MNRAS*, 419, 3571
- Geng A., Beck A. M., Dolag K., Bürzle F., Beck M. C., Kotarba H., Nielaba P., 2012b, *MNRAS*, 426, 3160
- Genzel R. et al., 2014, *ApJ*, 796, 7
- Girichidis P. et al., 2016, *MNRAS*, 456, 3432
- Han J. L., 2017, *ARA&A*, 55, 111
- Han J. L., Manchester R. N., van Straten W., Demorest P., 2018, *ApJS*, 234, 11
- Hanasz M., Otmianowska-Mazur K., Kowal G., Lesch H., 2009, *A&A*, 498, 335
- Haud U., 1981, *Ap&SS*, 76, 477
- Heald G. et al., 2015, Proc. Sci., Magnetic Field Tomography in Nearby Galaxies with the Square Kilometre Array. SISSA, Trieste, PoS#106
- Heesen V., Beck R., Krause M., Dettmar R.-J., 2011, *A&A*, 535, A79
- Heesen V., Brinks E., Leroy A. K., Heald G., Braun R., Bigiel F., Beck R., 2014, *AJ*, 147, 103
- Hernquist L., 1993, *ApJS*, 86, 389
- Hogan C. J., 1983, *Phys. Rev. Lett.*, 51, 1488
- Houde M., Fletcher A., Beck R., Hildebrand R. H., Vaillancourt J. E., Stil J. M., 2013, *ApJ*, 766, 49
- Hu C.-Y., 2019, *MNRAS*, 483, 3363
- Jacob S., Pfrommer C., 2017, *MNRAS*, 467, 1478
- Junk V., Walch S., Heitsch F., Burkert A., Wetzstein M., Schartmann M., Price D., 2010, *MNRAS*, 407, 1933
- Karademir G. S., Remus R.-S., Burkert A., Dolag K., Hoffmann T. L., Moster B. P., Steinwandel U. P., Zhang J., 2019, *MNRAS*, 487, 318
- Kazantsev A. P., 1968, Sov. J. Exp. Theor. Phys., 26, 1031
- Kazantsev A. P., Ruzmaikin A. A., Sokolov D. D., 1985, *JETP*, 88, 487
- Kim C.-G., Ostriker E. C., 2015, *ApJ*, 802, 99
- Kim K. S., Lilly S. J., Miniati F., Bernet M. L., Beck R., O'Sullivan S. P., Gaensler B. M., 2016, *ApJ*, 829, 133
- Kotarba H., Lesch H., Dolag K., Naab T., Johansson P. H., Donnert J., Stasyszyn F. A., 2011, *MNRAS*, 415, 3189
- Kraichnan R. H., 1968, *Phys. Fluids*, 11, 945
- Kulsrud R. M., Anderson S. W., 1992, *ApJ*, 396, 606
- Kulsrud R. M., Cen R., Ostriker J. P., Ryu D., 1997, *ApJ*, 480, 481
- Lahén N., Naab T., Johansson P. H., Elmegreen B., Hu C.-Y., Walch S., 2019, *ApJ*, 879, L18
- Lesch H., Hanasz M., 2003, *A&A*, 401, 809
- Malyshkin L., Kulsrud R. M., 2002, *ApJ*, 571, 619
- Miller M. J., Bregman J. N., 2013, *ApJ*, 770, 118
- Mishustin I. N., Ruzmaikin A. A., 1972, Sov. J. Exp. Theor. Phys., 34, 233
- Moss D., 1998, *MNRAS*, 297, 860
- Moster B. P., Macciò A. V., Somerville R. S., Johansson P. H., Naab T., 2010, *MNRAS*, 403, 1009
- Naab T., Ostriker J. P., 2017, *ARA&A*, 55, 59
- Niklas S., Beck R., 1997, *A&A*, 320, 54
- Niklas S., Klein U., Braine J., Wielebinski R., 1995, *A&AS*, 114, 21
- Pakmor R., Springel V., 2013, *MNRAS*, 432, 176
- Pakmor R. et al., 2017, *MNRAS*, 469, 3185
- Patrikeev I., Fletcher A., Stepanov R., Beck R., Berkhuijsen E. M., Frick P., Morellou C., 2006, *A&A*, 458, 441
- Powell K. G., Roe P. L., Linde T. J., Gombosi T. I., De Zeeuw D. L., 1999, *J. Comput. Phys.*, 154, 284
- Rieder M., Teyssier R., 2016, *MNRAS*, 457, 1722
- Rieder M., Teyssier R., 2017, *MNRAS*, 471, 2674
- Robishaw T., Quataert E., Heiles C., 2008, *ApJ*, 680, 981
- Roh S., Ryu D., Kang H., Ha S., Jang H., 2019, *ApJ*, 883, 138
- Röttgers B., Arth A., 2018, preprint ([arXiv:1803.03652](https://arxiv.org/abs/1803.03652))
- Ruzmaikin A. A., Turchaninov V. I., Zeldovich I. B., Sokoloff D. D., 1979, *Ap&SS*, 66, 369
- Ruzmaikin A. A., Sokolov D. D., Shukurov A. M., 1988a, *Astrophysics and Space Science Library, Vol. 133, Magnetic Fields of Galaxies*. Springer-Verlag, Berlin Heidelberg
- Ruzmaikin A., Sokolov D., Shukurov A., 1988b, *Nature*, 336, 341
- Schekochihin A. A., Cowley S. C., Hammett G. W., Maron J. L., McWilliams J. C., 2002, *New J. Phys.*, 4, 84
- Schekochihin A. A., Cowley S. C., Taylor S. F., Maron J. L., McWilliams J. C., 2004, *ApJ*, 612, 276
- Schleicher D. R. G., Beck R., 2013, *A&A*, 556, A142
- Schleicher D. R. G., Banerjee R., Sur S., Arshakian T. G., Klessen R. S., Beck R., Spaans M., 2010, *A&A*, 522, A115
- Shukurov A., 2000, Proceedings 232. WE-Heraeus Seminar, p. 191
- Shukurov A., Rodrigues L. F. S., Bushby P. J., Hollins J., Rachen J. P., 2019, *A&A*, 623, A113
- Somerville R. S., Davé R., 2015, *ARA&A*, 53, 51
- Springel V., 2005a, *MNRAS*, 364, 1105
- Springel V., 2005b, *MNRAS*, 364, 1105
- Springel V., Hernquist L., 2003, *MNRAS*, 339, 289
- Stein Y. et al., 2019, *A&A*, 623, A33
- Steinwandel U. P., Beck M. C., Arth A., Dolag K., Moster B. P., Nielaba P., 2019, *MNRAS*, 483, 1008
- Su K.-Y., Hayward C. C., Hopkins P. F., Quataert E., Faucher-Giguère C.-A., Kereš D., 2018, *MNRAS*, 473, L111
- Sun X. H. et al., 2015, *ApJ*, 811, 40
- Sur S., Shukurov A., Subramanian K., 2007, *MNRAS*, 377, 874
- Tabatabaei F. S., Krause M., Fletcher A., Beck R., 2008, *A&A*, 490, 1005
- Tabatabaei F. S., Berkhuijsen E. M., Frick P., Beck R., Schinnerer E., 2013, *A&A*, 557, A129
- Tabatabaei F. S., Mingué P., Prieto M. A., Fernández-Ontiveros J. A., 2018, *Nat. Astron.*, 2, 83
- Vazza F., Brunetti G., Brüggen M., Bonafede A., 2018, *MNRAS*, 474, 1672
- Widrow L. M., 2002, *Rev. Mod. Phys.*, 74, 775
- Wielebinski R., Krause F., 1993, *A&AR*, 4, 449
- Xu H., Li H., Collins D. C., Li S., Norman M. L., 2009, *ApJ*, 698, L14
- Zeldovich I. B., Ruzmaikin A. A., Sokolov D. D., 1983, *Magnetic Fields in Astrophysics*, Vol. 3. Gordon Breach Science Publishers, New York

This paper has been typeset from a Te<sub>X</sub>/L<sub>A</sub>T<sub>E</sub>X file prepared by the author.